Geochimica et Cosmochimica Acta 338 (2022) 34–53

Contents lists available at ScienceDirect

Geochimica et Cosmochimica Acta

journal homepage: www.elsevier.com/locate/gca

Extreme methane clumped isotopologue bio-signatures of aerobic and anaerobic methanotrophy: Insights from the Lake Pavin and the Black Sea sediments

Thomas Giunta [a,*], Edward D. Young [b], Jabrane Labidi [c], Pierre Sansjofre [d], Didier Jézéquel [c,e], Jean-Pierre Donval [a], Christophe Brandily [f], Livio Ruffine [a]

[a] Univ Brest, CNRS, Ifremer, Geo-Ocean, F-29280 Plouzané, France
[b] University of California Los Angeles, Department of Earth, Planetary and Space Sciences, CA 90095 Los Angeles, USA
[c] Université de Paris, CNRS, Institut de Physique du Globe de Paris, F-75005 Paris, France
[d] Sorbonne Université, CNRS, Muséum National d'Histoire Naturelle, IMPMC, 75005 Paris, France
[e] INRAE & Université Savoie Mont Blanc, CARRTEL, Thonon-les-Bains 74200, France
[f] Univ Brest, CNRS, Ifremer, BEEP, F-29280 Plouzané, France

ARTICLE INFO

Article history:
Received 23 February 2022
Accepted 26 September 2022
Available online 13 October 2022
Associate editor: Edward Hornibrook

Keyword:
Anaerobic oxidation of methane
Aerobic oxidation of methane
Methane clumped isotopes

ABSTRACT

Microbial methane oxidation - or methanotrophy - is a key control of the global methane budget on Earth, and perhaps in other planetary systems. Here, we explore the potential role of mass-18 isotopologues of methane, expressed as $\Delta^{13}CH_3D$ and $\Delta^{12}CH_2D_2$ values, in tracking both aerobic and anaerobic methanotrophy in nature. We examine two well documented methanotrophic environments: the Lake Pavin (France) water column, where methane degradation is dominated by aerobic methanotrophy (AeOM), and the Black Sea sediments (offshore Romania), dominated by anaerobic methanotrophy (AOM) coupled to sulfate-reduction. In both settings, lighter isotopologues are preferentially consumed, generating elevated $^{13}CH_4/^{12}CH_4$, $^{12}CH_3D/^{12}CH_4$, $^{13}CH_3D/^{12}CH_4$ and $^{12}CH_2D_2/^{12}CH_4$ ratios. This results in increasing of $\delta^{13}C$ and δD values in the residual methane for both settings, as observed commonly in systems dominated by methanotrophy. As a result, AeOM and AOM cannot be easily distinguished by the development of $\delta^{13}C$ and δD. In contrast, the $\Delta^{13}CH_3D$ and $\Delta^{12}CH_2D_2$ (departure from stochastic) values have opposite trajectories, with minimal decreases in the case of the AeOM-dominated system, but dramatic increases in the case of AOM, with $\Delta^{13}CH_3D$ and $\Delta^{12}CH_2D_2$ reaching values as high as 15.7 ‰ and 76.6 ‰, respectively. This contrasting behavior of clumped isotopologues signatures illustrates fundamental distinction between the two processes and the way they segregate methane isotopologues. These data demonstrate that both AeOM and AOM have distinctive kinetic isotope effects in natural settings, consistent with preliminary laboratory work. In particular, we find that γ-values (which measure the deviation to the product of 'normal' bulk isotope fractionation factors) are close to unity in the case of AeOM (*i.e.* a negligible clumped isotope effect), but significantly below unity in the case of AOM (*i.e.* strong clumped isotope effect). In addition, our data also illustrate how AOM under low-sulfate conditions may promote methane isotopologue equilibration. Taken together, we suggest these data and apparent isotopologue fractionation factors extrapolated from these two environments may help refine the potential bio-signatures of methane affected by methanotrophy.

© 2022 Elsevier Ltd. All rights reserved.

1. Introduction

Methane (CH_4) is the simplest reduced form of carbon and is presumably involved in biological reactions nearly since life appeared on our planet (Ciccarelli et al., 2006; Weiss et al., 2016; Russell and Nitschke, 2017). Although there are abiotic pathways for both production and degradation of methane, it is considered that most of methane cycling on Earth is biologically-mediated. Microbial methanogenesis (*i.e.* methane production) is an ubiquitous process and has been recognized in diverse range of anoxic environments, from wetlands and lakes (Borrel et al., 2012; Lopes et al., 2011), to marine and terrestrial sediments (*e.g.* Oremland and Taylor, 1978, Schoell, 1988; Martini et al., 2003;

* Corresponding author.
E-mail address: thomas.giunta@ifremer.fr (T. Giunta).

https://doi.org/10.1016/j.gca.2022.09.034
0016-7037/© 2022 Elsevier Ltd. All rights reserved.

Whiticar, 1999, Inagaki et al., 2015), to deep within cratonic basement rocks (*e.g.* Sherwood Lollar et al., 1993, Ward et al., 2004). Microbial methanogenesis is performed by a diverse group of Archaea referred to as methanogens, and is often the final step of organic matter degradation. On the other hand, microbial methanotrophy (*i.e.* methane degradation) may also be regarded as a terminal step of organic matter degradation, to the extent methane being produced is eventually oxidized into CO_2 or assimilated into cellular biomass. Methanotrophy is also a ubiquitous process, mediated by distinct communities of Bacteria and Archaea. The Aerobic Oxidation of Methane (AeOM) occurs by activity of a group of obligatory methanotrophic bacteria utilizing O_2 as the terminal electron acceptor (McDonald et al., 2008; Trotsenko and Murrell, 2008) as follows:

$$CH_4 + 2O_2 \rightarrow CO_2 + 2H_2O \quad (1)$$

Aerobic methanotrophy is the dominant pathway for methane oxidation in environments where oxygen is available such as in marine or lacustrine water columns (Schubert et al., 2006; Lopes et al., 2011; Oswald et al., 2016) or in soils and wetlands (Chowdhury and Dick, 2013). The Anaerobic Oxidation of Methane (AOM) is performed in anoxic conditions, mostly by Anaerobic Methane-Oxidizing Archaea (ANME). These microorganisms can catalyze AOM by reversing the CO_2 reducing methanogenesis pathway (Hallam et al., 2004), and may utilize, in syntrophy with other microbial partners, a variety of terminal electron acceptors including sulfate (Boetius et al., 2000; Orphan et al., 2001), nitrate (Raghoebarsing et al., 2006; Haroon et al., 2013) or metal oxides (Beal et al., 2009; Cai et al., 2018; Leu et al., 2020). The sulfate-dependent AOM was first to be recognized in shallow marine sediments, in pronounced Sulfate-Methane Transition Zones (STMZ), (Barnes and Goldberg, 1976; Iversen and Jorgensen, 1985; Alperin et al., 1988; Hoehler et al., 1994; Hinrichs et al., 1999) and is now considered to be a major methane sink in the oceans (Hinrichs and Boetius, 2002; Reeburgh, 2007). There, ANME thrive in synthrophy with sulfate-reducing bacterial partners, which result in the following net reaction:

$$CH_4 + SO_4^{2-} + H^+ \rightarrow CO_2 + HS^- + 2H_2O \quad (2)$$

The role of AOM mediated by microbial consortia has now been proposed and/or identified in many other environments such as in sedimentary gas reservoirs (Martini et al., 2003; Meng et al., 2017; Giunta et al., 2019), in lake sediments (Martinez-Cruz et al., 2017; Weber et al., 2017), in fracture fluids from cratonic rocks (Simkus et al., 2016; Lau et al., 2016; Warr et al., 2021) or in certain lakes as well as in marine water columns (Wakeham et al., 2003; Eller et al., 2005; Lopes et al., 2011). AOM is also considered as a plausible metabolism for life in the subsurface of Mars or Titan as well (Norman, 2011; Marlow et al., 2014; House et al., 2022). Overall, both AeOM and AOM metabolisms are considered critical processes for regulating the global methane budget on Earth. Therefore, it is crucial to develop tools to better identify and constrain the magnitude of these processes in the various natural settings where they might be at play.

Bulk carbon and hydrogen stable isotopes are commonly used to explore methane-based metabolisms. The methane bulk isotopic compositions for $^{13}C/^{12}C$ and D/H are expressed in ‰ relative to international standards according to the classic δ-notation:

$$\delta^{13}C = \frac{(^{13}C/^{12}C)_{sample}}{(^{13}C/^{12}C)_{VPDB}} - 1 \quad (3)$$

and

$$\delta D = \frac{(D/H)_{sample}}{(D/H)_{VSMOW}} - 1 \quad (4)$$

where VPDB is the Vienna Pee Dee Belemnite, and VSMOW is Vienna Standard Mean Oceanic Water. An empirical knowledge of 'typical' methanogenic or methanotrophic isotopic signatures as well as comparisons of isotope fractionation factors with those measured in laboratory cultures have been commonly used to explore both sources and sinks of methane in nature (*e.g.* Bernard et al., 1976; Schoell, 1988; Whiticar, 1999; Milkov and Etiope, 2018). However, in many instances, the co-existence of various sources of methane (whether biotic or abiotic) and of metabolisms at play can blur the isotopic signatures of these sources and sinks of methane, makings interpretation of the bulk isotope ratios challenging (*e.g.* Miller et al., 2016; Etiope, 2017). Furthermore, because the $\delta^{13}C$-CH_4 and δD-CH_4 crucially depend on the isotopic signatures of the carbon and hydrogen precursors, which are not necessarily identified nor accessible for sampling, the diagnosis of methane's origin remains challenging, especially in deep biosphere environments. What is more, isotope fractionations observed in nature often differ from those in laboratory studies (see Okumura et al., 2016 and reference therein).

Recently, advances in high-resolution mass-spectrometry and in laser adsorption spectroscopy allowed the measurement of the methane, 'clumped', doubly-substituted isotopologues $^{13}CH_3D$ (Stolper et al., 2014a; Ono et al., 2014; Young et al., 2016) and $^{12}CH_2D_2$ (Young et al., 2016; Eldridge et al., 2019; Gonzalez et al., 2019). This novel approach allows the investigation of isotope bond ordering in methane molecules. At thermodynamic equilibrium these relative abundances of multiply-substituted isotopologues depend on the temperature. The 'clumped' isotopologue compositions are reported versus a stochastic distribution (Wang et al., 2004), representing a perfectly random distribution of all of isotopes comprising all isotopologues that would occur at an infinite temperature, and expressed in per mil using the capital delta notation:

$$\Delta^{13}CH_3D = \frac{(^{13}CH_3D/^{12}CH_4)_{Sample}}{(^{13}CH_3D/^{12}CH_4)_{Stochastic}} - 1 \quad (5)$$

and

$$\Delta^{12}CH_2D_2 = \frac{(^{12}CH_2D_2/^{12}CH_4)_{Sample}}{(^{12}CH_2D_2/^{12}CH_4)_{Stochastic}} - 1 \quad (6)$$

In the 'clumped' systematic, Δ values are internally referenced to the stochastic distribution of the sample. This formalism for reporting the abundances of $^{13}CH_3D$ and $^{12}CH_2D_2$ has the advantage that it depends solely on the composition of methane itself. At equilibrium, these abundances reflect intra-species thermometers. So far, measurements of $\Delta^{13}CH_3D$ and $\Delta^{12}CH_2D_2$ have provided constraints on the temperature history experienced by methane in various geological contexts, from sedimentary environments dominated by thermogenic methane (*i.e.* thermocatalytic breakdown of organic matter) (Stolper et al., 2014b; 2015; 2017; Wang et al., 2015; Douglas et al. 2016; Young et al., 2017; Gruen et al., 2018; Giunta et al., 2019; 2021) to abiotic methane in hydrothermal systems (Wang et al., 2018; Labidi et al., 2020) or in cold crystalline environments (Wang et al.; 2015; Young et al., 2017). They are also useful as a means of tracing methane-based metabolisms. In laboratory cultures, both methanogens and methanotrophs appear to produce substantial disequilibrium signatures that could facilitate the recognition and quantification of these metabolisms (*e.g.* Stolper et al., 2015; Wang et al., 2015; Douglas et al., 2016; Wang et al., 2016; Young et al., 2017; Giunta et al., 2019; Ono et al., 2021). These exotic signatures have been recognized in certain natural environments, but there are numerous others where $\Delta^{13}CH_3D$ and $\Delta^{12}CH_2D_2$ instead seem to reflect a near-equilibration of the methane at environmental

temperatures, raising questions on how *in situ* substrate availability, growth rates and complex symbiotic ecosystems may affect clumped isotopologue signatures in nature.

The aim of this study is to further explore the distinction between AeOM and AOM as it manifests in the relative abundances of residual methane isotopologues. In particular, we aim to better characterize the isotopic effects associated with the narrow transition horizon between methanogenesis and methanotrophy. We investigate two well characterized natural settings: the meromictic Lake Pavin in central France, and shallow sediments from the Black Sea. Both settings display methanogenic to methanotrophic transition depth-profiles, though with different regimes of methanotrophy. The Lake Pavin water column is dominated by AeOM (Biderre-Petit et al., 2011; Lopes et al., 2011), whereas the Black Sea sediments show evidence of sulfate-dependent AOM (*e.g.* Jørgensen et al., 2001; 2004; Michaelis et al., 2002; Treude et al., 2005). In this study, we expand on concepts and ideas that have been developed by some recent studies (*e.g.* Yoshinaga et al., 2014; Wang et al., 2016; Ash et al., 2019) to explore on how methanotrophy may affect isotopic and isotopologue signatures, and how methane 'clumped' isotopologues might be used to identify and quantify the activity of these two metabolisms in natural environments.

2. Site description

2.1. Lake Pavin (France)

Lake Pavin is a meromictic crater lake located in the volcanic area of the Massif Central in France (Fig. 1). The crater's formation is associated with the most recent volcanic activity in the area (*ca.* 7000 years ago, see Chapron et al., 2010 and references therein) and is mostly composed of basaltic, trachyandesitic and granitic rocks. The lake is at an altitude of 1197 m above sea level and has a mean diameter of 750 m (area of 0.445 km^2) for a maximum depth (D_{max}) of 92 m. This particular geometry (great depth for limited surface area) has favored the development of permanent stratification (*i.e.* meromixis) of the lake water-column which is best evidenced by strong physico-chemical gradients with depth (*e.g.* temperature, conductivity, dissolved O_2) (Michard et al., 1994; Viollier et al., 1997; Lopes et al., 2011). In particular, the bottom layer of the lake (below ~60 m depth), also referred as the monimolimnion, is a dense and strictly anoxic layer that is presumably not affected by the seasonal mixing impacting the overlying waters (referred as mixolimnion). This deep layer is considered to be at steady-state (Viollier et al., 1997; Aeschbach-Hertig et al., 2002) and is home for elevated concentrations of reduced compounds, in particular methane, whose concentrations can reach as high as 4 mM at the bottom of the lake and up to 8 mM in the underlying sediment (Lopes et al., 2011; Borrel et al., 2012).

2.2. Black Sea sediment (offshore Romania)

The Black Sea is a marginal sea that bridges the European and Asian continents (Fig. 1). It is indirectly connected to the Atlantic Ocean through the Marmara and the Mediterranean Seas. The Black Sea was mostly composed of a freshwater lake during last Pleistocene glaciation and its reconnection to the open sea through the shallow Bosporus about 9000 years ago resulted in an inflow of (Atlantic) seawater, leading to its permanent water layer stratification. Freshwater is supplied by three main rivers, the Danube to the West, and the Dniepr and the Dniester to the North. These rivers deliver an important amount of organic carbon, the degradation of which has led to the enrichment of the water mass in hydrogen sulfide, making the Black Sea the largest anoxic basin on Earth. The west and the northwest parts of the Black Sea consist in a vast continental shelf bounded by the Danube and Dniepr river deltas. This vast sea is characterized by widespread seafloor methane-rich gas emissions from the river mouth to the deep basin (*e.g.* Reeburgh et al., 1991; Kessler et al., 2006; Pape et al., 2008). Accordingly, methane concentrations are generally elevated (up to several mM) in sediments and the water column. As per in other margin sedimentary environments, organoclastic sulfate reduction and methanogenesis are the dominant pathways for the degradation of organic matter in the sediment of the Black Sea (Jørgensen et al., 2001, Egger et al., 2016; Ruffine et al., 2021). The methane, and its links with the sulfur and iron cycles, among others, has been extensively investigated over the past decades through the

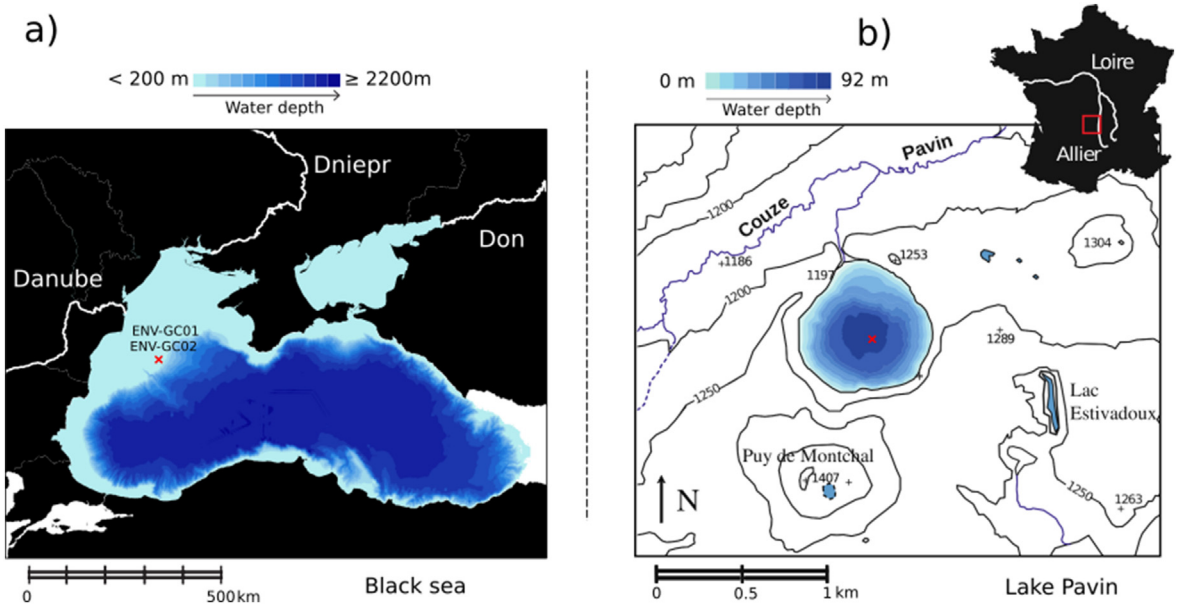

Fig. 1. a) Bathymetric map of the Black Sea with three of the tributaries and coordinates of the two gravity cores. b) Topographic and bathymetric map of the Lake Pavin in France, modified after Assayag et al., (2008) and Chassiot et al., (2018).

help of classical bulk isotopic tools (*e.g.* Jørgensen et al., 2001; 2004; Treude et al., 2005; Knab et al., 2009; Egger et al., 2016).

3. Methods

3.1. Sampling procedures

The main objective of this study is to measure the abundances of rare isotopologues of methane, $^{13}CH_3D$ and $^{12}CH_2D_2$, throughout vertical profiles where microbial methane oxidation is taking place. In order to put constraints on isotope fractionation factors associated to such reactions, one needs to measure isotopic compositions of methane over a large range of methane concentrations. Thus, being able to measure isotope ratios, especially clumped isotopologue ratios, in the main degradation intervals is challenging, because methane concentrations are low, necessitating the sampling of large volumes of water and/or of sediments in order to obtain the minimum amount of CH_4 required for analyses (>20 μmoles). Though the sampling procedures were different for the Lake Pavin (sampling of the water column) than for the Black Sea sediments (sub-sampling of fresh sediment cores), both procedures were adapted from well-described techniques for sampling methane for methane bulk isotopic ratio measurements ($\delta^{13}C$ and δD).

Lake Pavin sampling: The Lake Pavin water-column was sampled at different depths using a 20 L Niskin bottle from a barge located in the middle of the lake, where it reaches its greatest depth (~93 m). For each sampled depth, the filled Niskin bottle is recovered on the barge and allowed to overfill different type of glass bottles, some dedicated to methane concentration analyses, some dedicated to isotopic analyses. Samples for methane concentration measurements were collected in 160 mL borosilicate glass serum vials, and were quickly closed with blue butyl rubber stopper and aluminium seal. Depending on expected methane concentrations (based on Lopes et al., 2011), samples for isotopic analyses were collected in threaded boresilicate glass bottles of various sizes (from 150 to 2000 mL) and were quickly closed with butyl rubber stoppers and open screw caps. All water samples were then poisoned with 1 to 5 mL of saturated $HgCl_2$ solution, which was added through septa with a syringe and a connected open needle to allow purging an equivalent volume of sample. In laboratory, a helium head-space corresponding to ~20 % of the total volume was generated in each glass bottle. Meanwhile, the lake sediment was also sampled by using a UWITEC corer (D9 # L60 cm). The muddy sediment recovered from the core was then sub-cored between 40 and 44 cm and 48–52 cm depth with a 50 mL pre-cut plastic syringe and added to a 150 mL threaded glass bottle, then closed with massive butyl septa and open screw cap. Note that these sediment samples therefore had a head-space consisting of air.

Black Sea sampling: The Black Sea sediments were sampled during Envri Methane cruise (April 2019, https://campagnes.flotteoceanographique.fr/campagnes/18001189/) on board the R/V *Mare Nigrum* operated by GeoEcoMar Romania. The aim of the Envri Methane cruise was to develop a joint pilot experiment to measure methane transfer from the seafloor to the atmosphere (Grilli et al., 2021). Fresh sediments were sampled by gravity core at a water depth of *ca.* 110 m (Fig. 1a). Gravity cores GC-01 and GC-02 allowed the recovery of 139 and 142 cm of fresh sediment, respectively. Both cores were dedicated to the investigation of methane isotopologues in the pore-water column. On board, each core was cut into several sections, allowing sub-sampling of the sediment on fresh cut surfaces using 50 mL pre-cut plastic syringes. For each depth interval, a volume of 200 cm^3 of sediment or of 400 cm^3 was collected and rapidly put into a 500 mL or a 1000 mL borosilicate glass bottle (see Fig. S1 for more details). Samples were subsequently all poisoned with addition of 100 or 200 mL of NaOH (2 M) solution, before sealing the glass bottles with butyl rubber stopper and an open screw caps. Each glass bottle was then stored upside down at 4 °C. In the meantime, additional samples were also collected for analyses of dissolved species concentration in the pore-water, as well as for measuring the methane concentration. The sampling of pore waters for solute concentration analyses was achieved by using Rhizon samplers that were placed in the middle of each core section. Rhizon samplers consist of a hydrophilic porous polymer tube with an inner diameter of 2.5 mm and a length of 50 mm (Seeberg-Elverfeldt et al., 2005). The recovered pore-water, whose volume was generally between 5 and 15 mL, was then filtered (0.2 μm) and collected into a Nalgene bottle that was pre-acidified with 0.5 mL of HNO_3 (16 N). Meanwhile, sediment samples for the determination of the methane concentration as well of $\delta^{13}C$ values with Picarro analyzer were also collected, by adapting the standard IODP procedure (Andrén et al., 2015). Fresh sediment was sub-sampled with a 3 mL pre-cut plastic syringe and added into a 20 mL glass serum vial together with 8 mL of NaOH (2 M) solution. The serum vial is then rapidly sealed with a septum and an aluminum seal and stored upside down. The sediment sub-sampling for methane concentration measurement was done on fresh cut surfaces between each section (*i.e.* together with larger sub-sampled volumes for rare isotopologue analyses, see Supp.), whereas for GC-02, the sub-sampling was done at the same depth were the Rhizon samplers were installed.

3.2. Concentration measurements

Methane analysis were carried out by gas chromatography (Perichrom® Pr2250 and Pr2100) equipped with an FID detector and with manual injections for Lake Pavin samples and by autosampler (Dani HSS 86.50) for the Black Sea samples. Methane samples were left to equilibrate during at least 2 h at room temperature according to the procedure of Abril and Iversen, (2002) before analysis. Samples from the Lake Pavin were then quickly injected in the GC Perichrom Pr2250 using a Hamilton gastight sample lock 100 μL syringe. Head space samples from the Black Sea were heated to 60° C during 10 min with the DANI autosampler and then injected in the GC Pr 2100. For both types of samples, methane was separated on a Perichrom® Porapak Q (80/100 mesh) packed column with a length of 2 m and an internal diameter of 1/8 in.. The retention time for methane is 1.4 min. Once eluted, methane was burned inside the FID in a hydrogen/air flame at 250 °C. Analyses were recorded using the Winilab software. Methane concentrations were calculated using the solubility coefficients for methane from the literature (Yamamoto et al., 1976). The repeatability of measurements is 3 %. The limit of quantification for methane is of *ca.* 5 $nmol.L^{-1}$.

The dissolved oxygen (DO) profiles in the Lake Pavin were acquired with a multiparameter CTD probe (EXO 2), equipped with an optical O_2 sensor (optode). Calibration was performed for local saturation of 100 % O_2 in water vapor saturated air at lake surface pressure and response for 0 % sat. was checked in a 10 %wt solution of Na_2SO_3. The detection limit for dissolved O_2 is *ca.* 0.1 % or about 0.3 ± 0.2 μM.

3.3. Methane pre-concentration and purification

For samples collected for clumped isotope analyses, the methane was essentially 'diluted' in rather large head-space volumes dominated by He for the lake Pavin samples, or dominated by air for the Black Sea sediments. This required quantitative pre-concentration of the methane in smaller volumes for shipping and future analyses of clumped isotopes ratios at UCLA. We devel-

oped a vacuum line interfaced with a gas-chromatrograph (Agilent 7890A) equipped with a PorapakQ of 2 m length and a TCD at Ifremer. The sample is introduced onto the purification line via a purge-and-trap method. In this method, the entire volume of the head-space is flushed with a He carrier-gas (flow-rate of 80 mL/min) into a liquid nitrogen trap filled with active charcoal. The trap was designed in a U-shape using a stainless steel tube measuring 30 cm in length with a ¼ inch outside diameter. This rather large trapping volume was chosen to allow for quantitative trapping of methane, having in mind that air (N_2 + O_2) in head-space volumes of Black Sea samples would also partially condensate on active charcoal at liquid nitrogen temperature. Also, in order to avoid carrying too much moisture that could potentially form ice that would plug the line, the liquid nitrogen trap was preceded by a cylindrical volume filled with Drierite®. After 10 min of purging the sample head-space, the trap is isolated from the rest of the line and the He-excess is pumped. The trap is then warmed up to 80 °C and a secondary He carrier gas is used to flush (flow-rate of 25 m/min) the released towards GC which is warmed up at a constant temperature of 35 °C. The GC allows relatively good separation of air and methane. The peak of air starts eluting after 2 min and is flushed away, then the peak of methane is released after 5 min and is collected at the exit of the GC on a second liquid nitrogen trap (same design than first one) for 10 min. After isolation and pumping of He-excess in the second trap, the gas was finally transferred into an evacuated glass vial of 10 cc volume one third filled with active charcoal. Note however that for the Black Sea samples, the air content was too elevated for quantitative separation of methane and air in one single pass through the GC (air still being released at the time of methane elution), thus necessitating a second pass through the GC. In such case, the content of the second trap (mixture of air and methane) was thus transferred back to the first trap and then re-processed through the GC, allowing for complete separation of air and methane prior to collection of the methane in the evacuated glass tube of filled with active charcoal. At UCLA, these pre-concentrated (and purified) gas samples where purified once again on the lab vacuum line prior to introduction on the *Panorama*, following the standard UCLA method already outlined in Young et al., (2017).

3.4. Isotopologue ratio measurements

Picarro ($\delta^{13}C$): $\delta^{13}C$-CH_4 analysis were carried out with a G2201-i Cavity Ring-Down Spectrometer (CRDS) from Picarro (Santa Clara, USA) equipped with a Small Sample Isotope Module (SSIM) for low gas injections (between 25 and 100 µL). The instrument was used with the High Range (HR) mode and the gas volume was adjusted to have a methane concentration ranges between 10 and 1000 ppm at the CRDS cavity. Environmental gas samples analyzed in this study were injected directly inside the SSIM port using a gastight syringe (Brandily et al., 2021). Three certified $\delta^{13}C$-CH_4 gas standards of −23.9, −38.3 and −66.5 ‰ were used for the isotopic calibration of the CRDS analyzer (Isometric Instruments, Victoria, Canada). These gas standards are composed of methane diluted in hydrocarbon-free air. The CRDS analyzer was calibrated by injecting 5 replicates of 5 mL of certified $\delta^{13}C$-CH_4 gas standards with the help of gastight syringes (Hamilton) and Tedlar® sampling bags (Restek). The residual standard deviation for the $\delta^{13}C$-CH_4 is<0.4 ‰.

Panorama ($\delta^{13}C$, δD, $\Delta^{13}CH_3D$ and $\Delta^{12}CH_2D_2$): Methane gas samples were analyzed at UCLA to obtain methane isotopologue abundances. The ratios $^{13}CH_3D/^{12}CH_4$, $^{12}CH_2D_2/^{12}CH_4$, $^{13}CH_4/^{12}CH_4$, and $^{12}CH_3D/^{12}CH_4$ are measured with the prototype Nu Instruments Panorama, a high-resolution gas-source double-focusing mass spectrometer at UCLA. In order to measure $^{12}CH_4^+$, $^{13}CH_4^+$, $^{12}CH_3D^+$, $^{13}CH_3D^+$ and $^{12}CH_2D_2^+$ ion currents, the *Panorama* mass spectrometer is set to a mass resolving power equal to or greater than 40000. This allows resolving of the two mass-18 isotopologues ($^{13}CH_3D$ and $^{12}CH_2D_2$), both measured on the axial collector with an electron multiplier. Meanwhile, mass-16 and mass-17 isotopologues are measured on Faraday collectors with amplifier resistors of 10^{11} Ω. Sample and reference bellows are adjusted so that ion current intensities are balanced. The current intensities are rebalanced after each measurement cycle. At first, the magnet is set to measure simultaneously $^{12}CH_3D^+/^{12}CH_4^+$ and $^{12}CH_2D_2^+/^{12}CH_4^+$ ratios, with $^{12}CH_2D_2^+$ (18.04385 amu) being measured on the axial collector. In a second setting, the magnet is set to measure $^{13}CH_3D^+$ (18.04090 amu) on the axial collector, and $^{13}CH_4^+/^{12}CH_4^+$ and $^{13}CH_3D/^{12}CH_4^+$ ratios are measured simultaneously. Overall, the external 1σ error (n = 5) including both the accuracy and the reproducibility is estimated to be ±0.1 ‰ for $\Delta^{13}CH_3D$, ±0.8 ‰ for $\Delta^{12}CH_2D_2$, ±0.1 ‰ for $\delta^{13}C$, and of approximately ±0.3 ‰ for δD.

3.5. Reactive transport modeling

In order to infer isotope fractionation factors associated with methanotrophy, we developed a simple reactive transport model. We assume that at steady-state, the vertical distribution of the bulk methane concentration or of any of its isotopologue ($^{12}CH_4$, $^{13}CH_4$, $^{12}CH_3D$, $^{13}CH_3D$ or $^{12}CH_2D_2$) can be described by the general second order differential equation:

$$D_i^* \cdot \frac{\partial^2 C_i}{\partial x^2} + v \cdot \frac{\partial C_i}{\partial x} + R_i = 0 \quad (7)$$

where C_i is the methane isotopologue concentration of interest, D_i^* its effective diffusion coefficient taking into account the porosity structure and/or the tortuosity if diffusing in a porous medium like sediments (Boudreau, 1997) or eddy diffusivity in the water columns, v is the effective vertical velocity term, and R_i is the reaction rate for that isotopologue (source or sink). For modeling each methane isotopologue concentration with depth, we assume the reaction rates in the two settings can be described by a second-order rate equations. For the Lake Pavin waters we have.

$$R_i = k_i \cdot C_i \cdot C_{O_2} \quad (8)$$

and for the Black Sea sediments,

$$R_i = k_i \cdot C_i \cdot C_{SO_4^{2-}} \quad (9)$$

In these formulations, the rate constants are the only free parameters to be optimized in order to fit the data, and should be regarded as phenomenological rate constants for oxidation rather than as the constants for the elementary reaction steps comprising reactions (1) and (2). Reactive transport modeling is generally aimed at better quantifying and deciphering the various reactions rates affecting the methane and/or other dissolved compounds within the water or the sediment column (*e.g.* Lopes et al., 2011; Egger et al., 2016; 2017), and thus can require a more rigorous physical description of all potential reactions involving methane. However, the goal of the modeling performed here is to extract the effective isotope fractionation factors for these two distinct environments. Thus, simplifying the sinks of methane to a single, net oxidation reaction, is sufficient for this purpose. In each setting, the Eq. (7) is solved numerically for all isotopologues, using a finite difference method developed with a Python code. Two boundary conditions are defined as the two concentrations at the limits of the depth domain. At first, an effective rate constant for $^{12}CH_4$ (*i.e.* $^{12CH4}k$) is determined through least-square minimization between the model and the methane concentration profile where it is assumed that $^{12}CH_4$ concentrations are equal to bulk methane concentrations (a valid assumption given natural isotopic

abundances). Then, the effective rate constants for singly- and doubly-substituted isotopologues are optimized through least-square minimization between the model and the isotopic data, making use of the results for $^{12}CH_4$ and solving for the isotope fractionation factors according to $^{i}k = {}^{i}\alpha \cdot {}^{12CH4}k$.

4. Results

4.1. Lake Pavin water column and sediment

The water column was sampled at several discrete depths, from below the lake surface down to 90 m water depth (near the bottom of the lake). From the bottom, the methane concentration decreases across the monimolimnion over a 35 m depth profile and with minimal value of of 15 nM at measured at 51 m water depth. This methane concentration profile is consistent both in shape and amplitude with methane profiles published in previous studies (Lopes et al., 2011; Jézéquel et al., 2016). This indicates that the sampling protocol used here, which was required for collecting large volumes of water, did not yield measurable methane loss through degassing compared to more conservative syringe sampling methods (Lopes et al., 2011; Jézéquel et al., 2016). This is likely due to the low temperatures of the collected water (~4–5 °C), allowing methane to remain mostly soluble upon transfer from the Niskin bottle to the glass bottles. In contrast, the poor sediment cohesivity recovered through coring at the bottom of the lake did not allow precise measurement of the dissolved methane concentration in the sediment. Borrel et al., (2012) have reported concentrations ranging between 6 and 9 mM, thus significantly above the maximum concentration reported the water column.

In the water column, the methane $\delta^{13}C$ increases from −61 ‰ at 90 m depth ($[CH_4]$ = 4.08 mM) to −46 ‰ at 52 m water depth ($[CH_4]$ = 0.001 mM). With the exception of the sample LP-90, measurements of the $\delta^{13}C$ performed on the *Panorama* (together with other methane isotopologues) are all in good agreement with those performed on the *Picarro* analyzer (Fig. 2b). For sample LP-90 however, there is a shift of nearly 6 ‰ between the two measurement techniques. The reason for this poor agreement is unknown. However, given the relative homogeneity of the data measured on the *Picarro* for LP-90, LP-80, LP-70 and LP-60 (all with $\delta^{13}C$ near −60 ‰), and the good agreement with LP-70 and LP-60 measured on the *Panorama*, we suspect that for LP-90 sample, the methane may have undergone fractionation upon incomplete transfer on the purification line prior to measurement on the *Panorama*. Because it was not possible to replicate this measurement, the *Panorama* measurement for PV-90 must be considered with the caveat that it may be in error.

Measurements for methane δD, $\Delta^{13}CH_3D$ and $\Delta^{12}CH_2D_2$ were performed on the *Panorama* IRMS. The methane δD appears relatively stable at water depths of 90 m, 70 m and 60 m (despite the dubious measurement for PV-90), averaging −307 ± 3 ‰, and increases to −251 ‰ at 54 m water depth (conc. = 0.005 mM) (Fig. 2c). Meanwhile, $\Delta^{13}CH_3D$ and $\Delta^{12}CH_2D_2$ are rather stable at 60 and 70 m water depth, averaging 2.4 ± 0.4 ‰ and −17.6 ± 0.1 ‰ respectively, and decrease to 0.7 ‰ and −20.3 ‰ at 55 m water depth. Note that sample collected at 90 m shows the most positive $\Delta^{13}CH_3D$ and $\Delta^{12}CH_2D_2$ values in the water column, of 2.8 ‰ and −12.3 ‰ respectively. However, given the poor agreement for this sample between *Picarro* and *Panorama* measurements of $\delta^{13}C$, it is unclear how reliable these data are for this specific sample. The two samples collected from the lake sediment yield nearly identical methane isotopologue signatures, with $\delta^{13}C$ of −65 ‰, δD of −250 ‰ and $\Delta^{13}CH_3D$ and $\Delta^{12}CH_2D_2$ of about 5 ‰ and 7.9 ‰ respectively. Such methane isotopic composition in the sediment pore-waters is thus distinct from the methane collected in the water-column.

4.2. Black Sea sediments

The dissolved methane from Black Sea shallow sediments was analyzed at a few discrete depths in two distinct cores of 139 cm and 142 cm length. In both cores, the dissolved methane concentration is observed to decrease from bottom to top, with concentration reaching up to 2.2 mM in GC01 and 3.9 mM in GC02 at depth (Fig. 3a). Though generally consistent with previous studies on Black Sea shallow sediments (*e.g.* Jørgensen et al., 2001; Egger et al., 2016), our maximum CH_4 concentrations data are above methane saturation of *ca.* 1.3 mM at atmospheric pressure (calculated at 20 °C and salinity of 22 g/L following Mogollón et al., 2013) and yet below methane saturation at *in situ* subsurface condition (*ca.* 10 mM at 6 bars and 10 °C). Therefore, it is difficult to evaluate how much *in situ* dissolved methane may have been lost and to what extent the CH_4 concentrations presented here could be underestimated. The sulfate concentration profiles are nearly

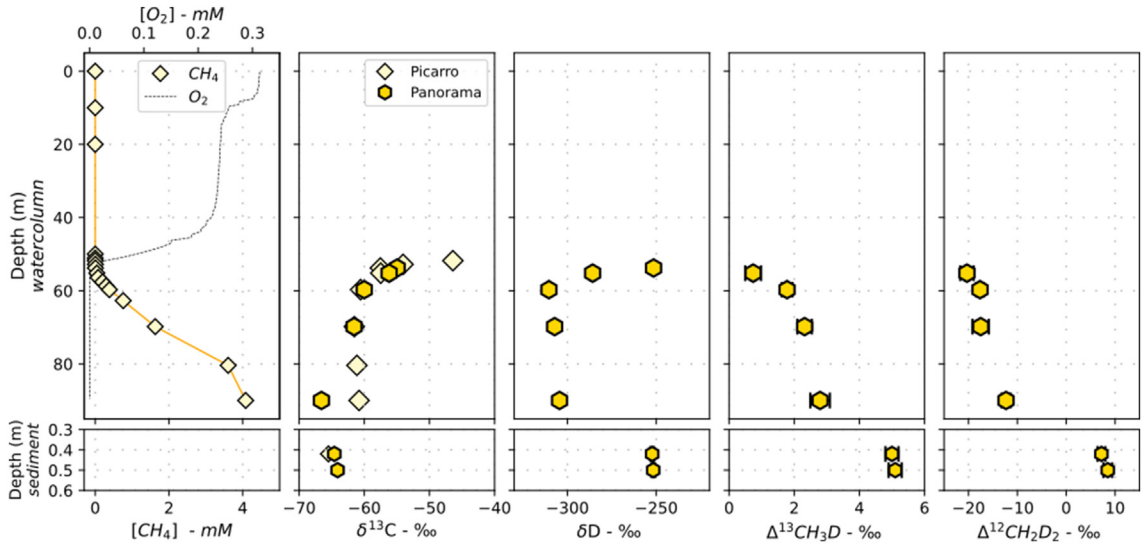

Fig. 2. Methane concentration and isotopic data (including doubly-substituted isotopologues) for the Lake Pavin. The methane concentration in the sediment was not measured in this study. Borrel et al., (2012) measured CH_4 concentrations in the first 40 cm of sediment that are ranging between 6 and 9 mM.

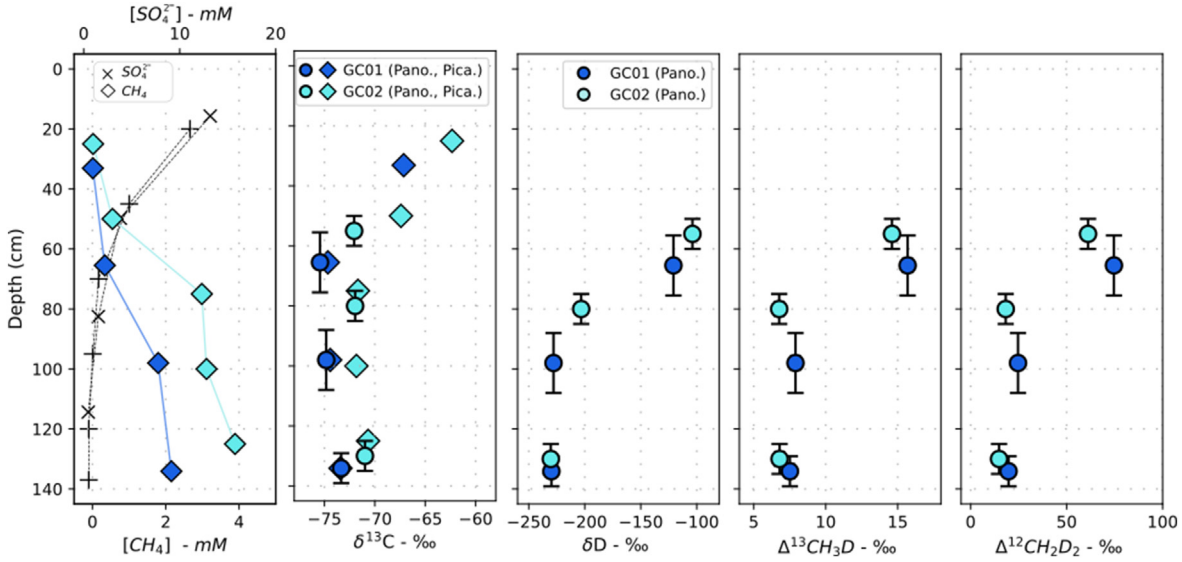

Fig. 3. Methane concentration and isotopic data (including doubly-substituted isotopologues) for Black Sea sediments. Errors bars reflect uncertainties of sampling depth (see Section 4.1. and Fig. S1).

identical in the two cores, decreasing from *ca.* 12 mM at 15 cm depth, down to *ca.* 0.5 mM in the deepest sampled horizon of each cores. Thus, albeit limited in overall recovered lengths, the two cores collected for this study are successfully capturing the SMTZ, occurring at *ca.* 40–100 cm depth.

The two cores share similar methane isotopic features. Measurements on the *Picarro* analyzer reveal relatively homogeneous $\delta^{13}C$ below *ca.* 60 cm depth in each cores, averaging − 74.2 ± 0.7 ‰ (n = 3) in GC01 and −71.4 ± 0.6 ‰ (n = 3). The $\delta^{13}C$ then increases to −67.1 ‰ at 33 cm in GC01 and to −62.3 ‰ at 25 cm in GC-02. The *Panorama* measurements of $\delta^{13}C$ on 6 samples collected at similar depth intervals all yielded consistent values (Fig. 3b), with perhaps one exception for the sample collected at the 50–60 cm depth interval in GC02. There, $\delta^{13}C$ is different by 4.6 ‰ compared to the sample collected at 50 cm depth and measured on the *Picarro* analyzer. We suggest this apparent discrepancy is due to the nature of the sampling. The sample for clumped isotopes integrates all methane contained in the sediment pore water over a 10 cm length (*i.e.* the length of the 50 cc syringe used for sediment sub-sampling, see Fig. S1). Therefore, given the overall CH_4 concentration profile (*i.e.* increasing with depth) and the fact that $\delta^{13}C$ values measured below this depth interval all point towards $\delta^{13}C$ values in the vicinity of −71 ‰, we suggest the measured $\delta^{13}C$ value simply represents the isotopic composition of the methane integrated between 50 and 60 cm depth. Unfortunately, our sampling resolution – which was primarily dictated by the need to collected enough methane – does not allow to establish how sharp the isotopic transition is at the location of sampling. Overall, the apparent consistency of other δD, $\Delta^{13}CH_3D$ and $\Delta^{12}CH_2D_2$ data between the two cores (see below) suggests that the bulk and clumped isotope values for the sample collected at the 50–60 cm depth interval in GC02 are valid.

The *Panorama* measurements of δD, $\Delta^{13}CH_3D$ and $\Delta^{12}CH_2D_2$ further demonstrate the similarity of the methane isotopic profiles between the two cores. The δD increases from −230 ‰ at the base of the SMTZ in the two cores (*ca.* 130 cm depth) to −121 ‰ in GC01 at the 55–75 cm depth interval and to −104 ‰ in GC02 at the 50–60 cm depth interval. Note this range of variations for δD in the Black Sea sediments is consistent with the data reported by Egger et al. (2016) in the Western part of the Black Sea. In both cores, $\Delta^{13}CH_3D$ and $\Delta^{12}CH_2D_2$ show limited variations in the deepest sampled intervals, averaging 7.2 ± 0.6 ‰ and 19.4 ± 4 ‰ respectively, and exhibit dramatic increases in the shallowest intervals, with values as high as 15.7 ‰ and 74.6 ‰ respectively for GC01, and as high as 14.6 ‰ and 61.1 ‰ respectively for GC02.

4.3. Near-equilibrium and disequilibrium signatures among microbially-mediated methane

When a sample reflects thermodynamic equilibrium, both mass-18 isotopologue yield concordant temperatures and the gas sample plots on the equilibrium curve in the $\Delta^{13}CH_3D$-$\Delta^{12}CH_2D_2$ space. In natural samples, whether an equilibrium temperature reflects a methane formation or re-equilibration is currently a subject of investigation. On the other hand, samples plotting off the equilibrium curve may reflect kinetics and/or reservoir effects associated with methane synthesis, or perhaps other secondary processes such as mixing, diffusion, or partial degradation of methane. On the basis of $\Delta^{13}CH_3D$ and $\Delta^{12}CH_2D_2$ signatures, we identified three groups with specific patterns. A first group of samples, coming from the sediment of the Lake Pavin and from the lower part of the SMTZ in the Black Sea sediments, are near-equilibrium low-temperature region, and bear striking resemblance to other methane-based ecosystems found in marine or continental sediments (Fig. 4). The second group of samples is composed of the four samples from Lake Pavin water-column, with negative $\Delta^{12}CH_2D_2$ values down to –22 ‰. These signatures reflect disequilibrium and are similar to microbial methane produced in the laboratory (*e.g.* Young et al., 2017; Giunta et al., 2019) and methane of microbial origin from boreal lakes (Young, 2019) (Fig. 4). Lastly, a third group of samples is defined by the two samples collected in the SMTZ horizon of the Black Sea sediments, and show extremely enriched $\Delta^{13}CH_3D$ and $\Delta^{12}CH_2D_2$ values. These samples also reflect disequilibrium, and represent to date, the most positive values ever reported for clumped isotopologues in a natural setting.

5. Discussion

5.1. The ambiguity of 'pristine' signatures of methanogenesis

In both settings investigated here, the methane found at the bottom of each depth-profile is deriving from microbial methanogenesis. In Lake Pavin, methane is produced both at the bottom of

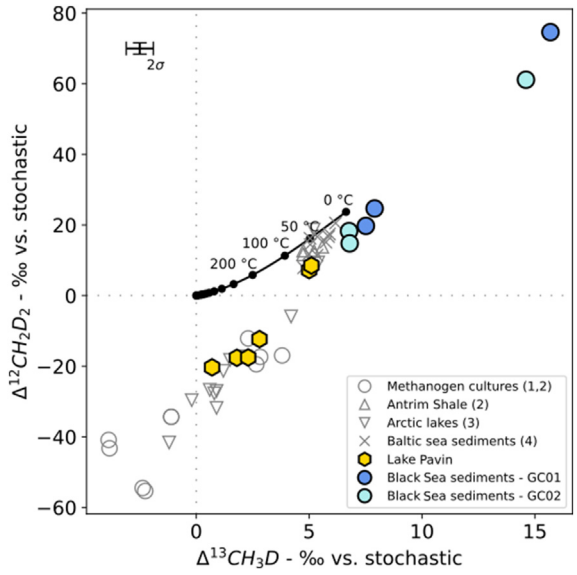

Fig. 4. Data reported in the clumped isotopologue space. The thermodynamic equilibrium line (black) is calculated after correlations developed by Young et al. (2017). Other reported data are from (1): Young et al., (2016); (2): Giunta et al., (2019); (3): Young, (2019); (4): Ash et al., (2019).

the water-column through hydrogenotrophic methanogenesis and in the sediment through a mix of hydrogenotrophic and acetoclastic methanogenesis (Biderre-Petit et al., 2011; Lopes et al., 2011). Yet, these two presumed production reservoirs show very distinct bulk and clumped isotope signatures. The large offsets from $\Delta^{13}CH_3D$-$\Delta^{12}CH_2D_2$ equilibrium observed in the lower part of the water-column resemble those measured on methane produced by hydrogenotrophic methanogens in the laboratory (Young et al., 2017; Giunta et al., 2019; Fig. 4). It is worse noting that bulk isotope fractionation between CH_4-δD and water-δD (ranging from *ca.* −50 to −56 ‰, Gal et al., 2015) would also illustrate such an isotope fractionation typical of methanogenic growth (*e.g.* Wang et al., 2015; Gruen et al., 2018). Taken together, these observations support genome-based studies suggesting that the hydrogenotrophic pathway is the main production route for methane in the water-column (Biderre-Petit et al., 2011). In sharp contrast, the two samples collected in the Pavin sediment, are plotting much closer to the equilibrium line, at odds with expectations based on laboratory cultures for a system dominated by microbial methanogenesis. In the Black Sea sediments, the production of methane is thought to primarily derive from hydrogenotrophic methanogenesis. The four samples from the lower part of the SMTZ show signatures close to clumped isotopologue equilibrium, with average $\Delta^{13}CH_3D$ and $\Delta^{12}CH_2D_2$ values of 7.2 ± 0.6 ‰ and 19.4 ± 4 ‰. These values translate in apparent temperatures of -14^{+15}_{-14}°C and 26^{+29}_{-24}°C, statistically indistinguishable from *in situ* temperature of *ca.* 10 °C.

Our data illustrate the complexity of the information captured by the of clumped signatures for microbial methanogenesis in nature. In many environments where microbial methanogenesis is presumed to be the dominant methane-based metabolism, the clumped isotopologues appear to reflect near-equilibration production of the methane, at odds with disequilibrium signatures systematically observed in laboratory cultures, regardless of the pathway involved. This near-equilibration behavior appears especially visible among what Okumura et al., (2016) call 'aged methane': meaning in hydrogeological environments that are isolated enough to accumulate methane over geological time, for instance in deep sea sediments (Wang et al., 2015; Douglas et al., 2016; Inagaki et al., 2015; Ijiri et al., 2018) or in some continental sedimentary gas reservoirs (Stolper et al., 2015). The isotopic discrepancy between 'aged methane' and laboratory methane may reflect the rate of methanogenesis (Wang et al., 2015; Stolper et al., 2015; 2017; Douglas et al., 2016; 2020; Gropp et al., 2022). Accordingly, large substrate availability (and thus free energy) in laboratory cultures would dominate kinetic effects for methane isotopologues, yielding disequilibrium abundance of isotopologues, whereas lower substrate availability, perhaps typical of the deep biosphere, would result in lower rates of methanogenesis and thereby in isotopic signatures that are controlled by thermodynamic equilibrium rather than kinetics. In line with this hypothesis, isotopologue disequilibrium at the bottom of the Pavin water-column could reflect the expression of *fast* methane production (perhaps promoted by continuous delivering of fresh labile organic matter into the lake), whereas near-equilibrium signatures in the Pavin sediment or from the lower part of the SMTZ in the Black Sea would reflect *slower* methanogenesis resulting from *more limited* nutrient availability. Note this hypothesis currently still lacks a clear experimental validation. Experiments under low hydrogen (H_2) partial pressures suggest that microbial methane could form closer to thermodynamic equilibrium, but still far from what is observed in nature on 'aged' methane (Okumura et al., 2016; Douglas et al., 2020). This may reflect the challenge of reproducing the (presumably) extremely low methanogenesis rates of the deep biosphere in the laboratory.

An alternative hypothesis for explaining these near-equilibrium signatures is that they instead reflect the interplay of different metabolisms in natural ecosystems. In particular, it has been proposed that micro-organisms involved in AOM may in energy-limited environments contribute to reprocess microbial methane towards thermodynamic equilibrium (Yoshinaga et al., 2014; Young et al., 2017; Young, 2019; Giunta et al., 2019; Ash et al., 2019; Warr et al., 2021, Wegener et al., 2021; Ono et al., 2021; 2022; Gropp et al., 2022). Note this hypothesis has some experimental validation: AOM coupled to sulfate-reduction appears to at least partially drive the residual methane towards isotopic equilibrium (Yoshinaga et al., 2014; Young, 2019; Wegener et al., 2021). The exact interplay of methanogenesis and AOM and the net resultant on isotopic signatures in conditions representative of the deep biosphere is still under investigation however (Ono et al., 2022). In the Black Sea sediments, the widely documented presence of ANME (*e.g.* Michaelis et al., 2002; Knittel et al., 2005; Treude et al., 2005) may argue in favor of this *reprocessing* hypothesis for explaining the near-equilibrium values observed at the base of the SMTZ (we will explore this further in Section 5.3.3). In the Lake Pavin sediment however, 16S rRNA analyses identified the presence of known methanogens (*Methanosaetaceae* and *Methanomicrobiales*) but not of ANME nor of related lineages (Lehours et al., 2007; Borrel et al., 2012). Yet, genomic analyses have also revealed that the archeal community in Lake Pavin sediment is largely dominated (>70 %) by uncultured archeal lineages of the Marine Benthic Groupe-D (MBG-D). The metabolisms of the MBG representatives are mostly unknown, but their ubiquitous presence in methane-rich environments suggest their potential role in methane cycling (Beal et al., 2009; Zhou et al., 2019). In particular, the presence of MBG members in habitats where AOM occurs, whether in wetlands (Valenzuela et al., 2017), in lakes (Schubert et al., 2011) or in marine sediments (Inagaki et al., 2006; Beal et al., 2009; Webster et al., 2011), suggest they may be involved in methanotrophy. Whether they could contribute, as ANME, to (partial) re-equilibration of microbial methane is currently unknown, but could offer an explanation for near-equilibrium signatures of the methane in the sediment of Lake Pavin.

5.2. The effects of methanotrophy on methane isotopologues

Both settings exhibit typical methanotrophic transitions, with methane concentrations decreasing from *ca.* 4 mM at depth to near 0 mM, consistent with the methane being progressively consumed as it is transported upward. In both settings, the bulk $\delta^{13}C$ and δD values of the methane increase along with the decrease in methane concentration, which is *a priori* consistent with either AeOM or AOM processes, both kinetically favoring the degradation of lighter isotopologues (*e.g.* Coleman et al., 1981; Alperin et al., 1988; Holler et al., 2011; Feisthauer et al., 2011). However, the rare isotopologues behave differently for the two settings. The $\Delta^{13}CH_3D$ and $\Delta^{12}CH_2D_2$ values decrease with lower methane concentrations in the Lake Pavin water column dominated by AeOM, whereas they show dramatic increases in the Black Sea sediments dominated by AOM (Figs. 2 and 3). Importantly, our data from the Black Sea suggest that AOM is capable of producing strong disequilibrium effects on the residual methane, as evidenced by the extraordinarily elevated $\Delta^{13}CH_3D$ and $\Delta^{12}CH_2D_2$ values measured here. This observation is consistent with first experimental observations (Ono et al., 2021), but contrast with recent field-based observations in the Baltic sea where AOM was interpreted to produce equilibrium among methane clumped isotopologues (Ash et al., 2019).

Taken together, these data illustrate how AeOM and AOM yield vastly different methane isotopologue signatures. Methane isotopologue signatures could provide useful constraints on the type of methane consumption operative in nature.

5.3. Inferring in situ fractionation factors of methanotrophy

The expression of contrasting behaviors of methane isotopologues during methanotrophy must reflect different isotope fractionation factors at play in these environments. In the case of methanotrophy, isotope fractionation factors correspond to the relative rate constant of a heavy isotopologue (whether $k^{13}CH_4$, $k^{12}CH_3D$, $k^{13}CH_3D$ or $k^{12}CH_2D_2$) to the rate constant of the light, non-substituted, isotopologue (*i.e.* $k^{12}CH_4$). In the following, fractionation factors for bulk carbon isotopes and for bulk hydrogen isotopes, as well as for 'clumped' isotopologues are referred as $^{13}\alpha$, $^{D}\alpha$, $^{13D}\alpha$ and $^{D2}\alpha$ respectively. Basic kinetic considerations suggest that α values should be <1 for methanotrophy in which there is a preferential consumption of the lighter $^{12}CH_4$ isotopologues. In laboratory cultures or incubations of methanotrophic organisms, derived fractionation factors vary considerably, with $^{13}\alpha$ ranging between 0.971 and 0.997, and $^{D}\alpha$ ranging from 0.680 to 0.906 (*e.g.* Coleman et al., 1981; Templeton et al., 2006; Kinnaman et al., 2007; Feisthauer et al., 2011; Rasigraf et al., 2012; Ono et al., 2021). Note that when extrapolated from natural environments, kinetic isotope fractionation factors often tend to be closer to 1, representing less of a kinetic fractionation. For example, $^{13}\alpha$ values of 0.996 and $^{D}\alpha$ values of 0.952 have been reported (*e.g.* Happell et al., 1994).

Fractionation factors for 'clumped' isotopologues of methane are less constrained, in particular for $^{12}CH_2D_2$. In the limit where isotopes distribute stochastically across isotopologues, the fractionation factors for doubly-substituted isotopologues would simply be the product of the bulk fractionation factors, following the "rule of the geometric mean" (Bigeleisen, 1955). This is the result at thermodynamic equilibrium at high temperatures where the isotope exchange equilibrium constants are simply the ratios of symmetry numbers. However, the few studies on methane clumped isotopologues have shown that this is not the case in general, especially in the oxidation reactions where bond rupture is involved (Whitehill et al., 2017; Haghnegahdar et al., 2017; Ono et al., 2021). This may lead to fractionation factors for clumped isotopologues that deviate significantly from the product of bulk isotope fractionation factors. The γ coefficient has been introduced as a means of quantifying this departure from the rule of the geometric mean (Wang et al., 2016) and to define $^{13D}\alpha$, the fractionation factor for $^{13}CH_3D/^{12}CH_4$ as

$$^{13D}\alpha = \frac{k_{13CH_3D}}{k_{12CH_4}} = {}^{13}\alpha.{}^{D}\alpha.{}^{13D}\gamma \quad (10)$$

where $^{13D}\gamma$ is an empirical parameter that can be adjusted to fit experimental or field data and would reflect the intrinsic 'clumped' effect for $^{13}CH_3D$ isotopologue. Similarly, $^{D2}\alpha$, the fractionation factor for $^{12}CH_2D_2/^{12}CH_4$, can be described as.

$$^{D2}\alpha = \frac{k_{12CH_2D_2}}{k_{12CH_4}} = {}^{D}\alpha.{}^{D}\alpha.{}^{D2}\gamma \quad (11)$$

where $^{D2}\gamma$ is an empirical parameter reflecting the intrinsic 'clumped' effect for the $^{12}CH_2D_2$ isotopologue. When γ coefficients equal unity, the fractionation factor for the multiply-substituted isotopologue simply corresponds to the product of bulk isotope fractionation factors. So far, laboratory cultures of *Methylococcus capsulatus* performing AeOM have revealed an absence of an intrinsic 'clumped' isotope effect with $^{13D}\gamma \sim 1$ (Wang et al., 2016), whereas recent AOM experiments by ANME (Ono et al., 2021) have revealed $^{13D}\gamma$ values significantly lower than unity. Note that the magnitude of the γ exerts a fundamental control on whether $\Delta^{13}CH_3D$ and $\Delta^{12}CH_2D_2$ values of a methane experiencing methanotrophy become more positive or more negative. Below, we derive apparent isotope fractionation factors through simple 1-D reactive transport modeling of these two settings.

5.3.1. Lake Pavin water-column, AeOM methanotrophy

In the Lake Pavin, the methane oxidation occurs at a water depth ranging between 50 and 60 m (Lopes et al., 2011). Below 60 m, the distribution of methane concentration and isotopologue ratios must be essentially controlled by turbulent diffusion. Contrasting with a pure diffusion process, turbulent or eddy diffusion is "non-fractionating" for entrained isotopologues. In the bottom part of the Lake Pavin water column, the eddy diffusivity is low, inferred to be in the order of 1–20 $m^2.yr^{-1}$ (Aeschbach-Hertig et al., 2002), which is only one to two order of magnitudes greater than typical diffusion coefficients of a dissolved substance in water (in the range of 0.1 $m^2.yr^{-1}$), so it is conceivable that molecular diffusion could be expressed.

In order to infer the apparent fractionation factors associated with methanotrophy in Lake Pavin, we modeled the concentration of all methane isotopologues as described in Section 3.5. Our model fits the Lake Pavin water column concentration and isotopic profiles (Fig. 5) with net degradation rates that are consistent with Lopes et al., (2011), showing a peak near 55 m depth of *ca.* 0.4 $mM.yr^{-1}$. The model carbon and hydrogen bulk isotope fractionation factors are of rather low magnitude, with $^{13}\alpha$ = 0.9978 (or *ca.* 2.2 ‰) and $^{D}\alpha$ = 0.9610 (or *ca.* 33.9 ‰), placing them at the lower end of all fractionation factors reported so far for AeOM whether in laboratory cultures or in field studies (Fig. 6). Note that accounting for a diffusion isotope effect would change each magnitude of fractionation factors by about 0.003 (*i.e.* 3 ‰) (Fig. S3). Fractionation factors for clumped isotopologues are off small magnitude as well, with $^{13D}\alpha$ = 0.9608 and $^{D2}\alpha$ = 0.9261. For comparison, pure AeOM in laboratory cultures have resulted in $^{13D}\alpha$ values ranging between 0.7804 and 0.8847 (Wang et al., 2016, note there was no available $^{12}CH_2D_2$ data in this study). Importantly, these fractionation factors for clumped isotopologues are indistinguishable from the product of bulk isotope fractionation factors, with $^{13D}\gamma$ = 1.0021 ± 0.0026 and $^{D2}\gamma$ = 1.0029 ± 0.003 7. This observation is consistent with the results of Wang et al.,

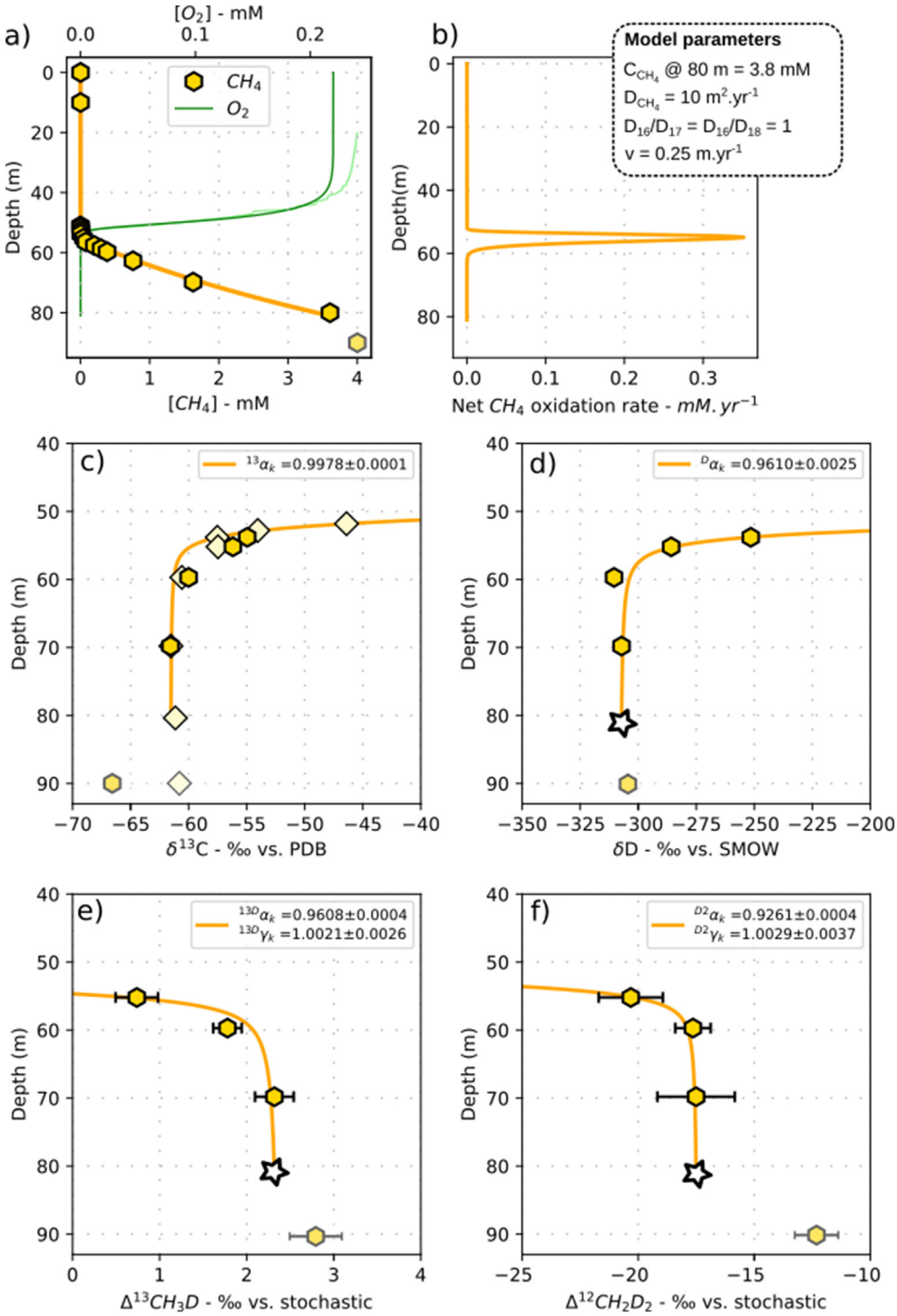

Fig. 5. Inferring apparent isotope fractionation factors associated to methane degradation in the Lake Pavin water-column with a reactive transport model. In order to avoid considering microbial methane production in the lower part of the water column, the transport-degradation model is solved down to 80 m water depth only. We assumed δD, $\Delta^{13}CH_3D$ and $\Delta^{12}CH_2D_2$ signatures at 80 m water depth to be identical to 70 m depth. A reasonable assumption given that at this depth interval the methane and its isotopologue distributions are solely controlled by non-fractionating transport processes (Lopes et al., 2011). The turbulent diffusion coefficient is set to 10 $m^2.yr^{-1}$, an average value between maximum and minimum values inferred for the monimolinion (1.6 to 19 $m^2.yr^{-1}$, Aeschbach-Hertig et al., 2002). The vertical fluid flow velocity is set to 0.25 $m.yr^{-1}$, scaling with the area of the lake at 60 m water depth and an estimated 1.6 $L.s^{-1}$ vertical flow (Assayag et al., 2008).

(2016) on $^{13}CH_3D$ isotopologue, and could be a fingerprint of AeOM metabolisms in nature.

It is difficult to categorically explain the small magnitude of fractionation factors obtained from the Lake Pavin data, although we note it is generally consistent with the fact that α values determined from the field are often *smaller* than in the laboratory (Fig. 6). In a reactive-transport model, transport parameters such as diffusion coefficients and/or advection rates (treated here as input parameters) may in principle affect the derived model isotope fractionation parameters. Sensitivity analyses performed for a range of D and v values did not yield significantly different results, however (Fig. S3). The values derived here may thus

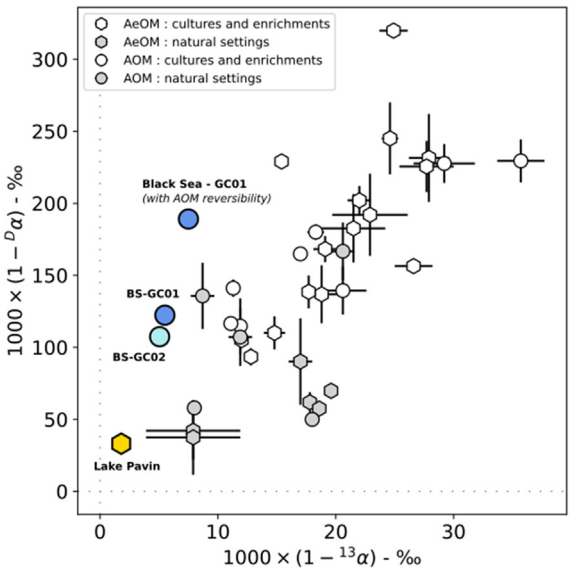

Fig. 6. Comparison of bulk isotope fractionation factors ($^{13}\alpha$ and $^{D}\alpha$) derived from reactive transport modeling, with values extrapolated for AOM or AeOM in laboratory or from field measurements (Coleman et al., 1981; Happell et al., 1994; Kinnaman et al., 2007; Feisthauer et al., 2011; Holler et al., 2011; Rasigraf et al., 2012; Wang et al., 2016; Ono et al., 2021).

accurately capture the *in-situ* fractionation factors for this setting. Experimental works suggest that the absolute magnitude of isotope fractionation upon AeOM may be controlled by CH_4 transport across cell membranes or by the form of the enzyme (the methane monooxygenase - MMO) the CH_4 is binding to (*e.g.* Summons et al., 1994; Templeton et al., 2006; Feisthauer et al., 2011). Importantly, chemostat experiments by Templeton et al., (2006) clearly demonstrated that a single type of methanotrophic bacteria may produce apparent $^{13}\alpha$ values varying widely, from 0.997 (*ca.* 3 ‰) to 0.962 (*ca.* 38 ‰), as a function of cell density. Accordingly, under high cell density and high concentration of MMO enzymes, the diffusion of methane across cell membranes may become a rate-determining step. This would mask the intrinsic fractionation factor associated with oxidation of methane by MMO enzymes and result in *smaller* apparent fractionation factors (Templeton et al., 2006). In the Lake Pavin water-column, the important methane flux contributes to elevated concentrations of methanotrophic bacteria, with cell densities as high as 10^5 cell·mL^{-1} at *ca.* 50–60 m depth (Lehours et al., 2007). Thus, although it seems difficult to evaluate how the chemostat experiments would scale (in terms of cell densities and absolute rates) to the Lake Pavin water column, the mechanism proposed by Templeton et al. (2006) may offer a partial explanation for the rather low fractionation factors derived from the natural data here. Future studies that include carbon isotope signatures of the associated biomass and DIC may help to validate this hypothesis with additional mass balance constraints.

5.3.2. Black Sea sediments, AOM methanotrophy

Solving the reactive transport equation in the Black Sea sediments is more challenging because of the large uncertainties regarding the dissolved methane concentration profiles. This is partly due to the poor sampling resolution, a direct consequence of sampling large volumes of sediments for clumped isotope analyses. It is also likely that dissolved methane has escaped from the samples between the time of the coring and the onboard subsampling of fresh sediment into the head-space vials. For comparison, complete bio-geochemical modeling of the methane concentration profile in the Romanian sector of the Black Sea point towards CH_4 concentrations of about 4 to 5 mM below the SMTZ (at sulfate concentration equivalent to those measured here at the base of each core), and even up to 15 mM in deeper sections of the sediments (Egger et al., 2016). Here, we tested two different scenarios with distinct boundary conditions for modeling the CH_4 concentration profiles (see details in Fig. 7). Independently of which scenario is used, our model results in maximum degradation rates located between 80 and 100 cm depth in the two cores; only the amplitude of the degradation rate varies (Fig. 7b). Importantly, inferred fractionation factors are quite insensitive to the scenario chosen and nearly identical in the two cores (Fig. S4 and S5), all resulting in largely positive $\Delta^{13}CH_3D$ and $\Delta^{12}CH_2D_2$ values such as measured here. Bulk isotope fractionation factors extrapolated are of higher magnitude than those extrapolated in the Lake Pavin, but still on the low end of values reported so far in the literature for microbial AOM processes, especially for carbon isotopes (Fig. 6). For $^{13}CH_3D$ isotopologue, we infer $^{13D}\alpha$ values of 0.8676 and 0.8817, which compare positively in terms of magnitude with those determined in AOM cultures, ranging between 0.764 and 0.869 (Ono et al., 2021). Lastly, we note that the $^{13D}\gamma$ and $^{D2}\gamma$ that we retrieved from our models are persistently below unity, with values of 0.9929 (GC01) and 0.9939 (GC02), and 0.9462 (GC01) and 0.9546 (GC02), respectively. Despite the large uncertainties associated with these numbers, this observation is consistent with the $^{13D}\gamma$ values of 0.9872 and 0.9952 in AOM incubations (Ono et al., 2021, note that $^{12}CH_2D_2$ was not measured in their study). We note however that this reactive transport modeling does not achieve a perfect fit with the isotopic profiles. In particular, the model fails to produce the isotopic homogeneity observed at the bottom of each profile (Fig. 7c, d, e and f). Taken at face value, the observed homogeneous isotopic signatures would instead suggest that there is limited methane oxidation. This seems to be in contradiction with the modeled CH_4 concentrations and the resulting degradation rate profiles (Fig. 7b) instead suggesting that methane is already being consumed at the base of each sediment profiles. This apparent discrepancy between modeled isotopic data and net degradation rates may simply result from our poor sampling resolution and incorrect evaluation of the *true* CH_4 concentration profile in the sediment. Yet for exploratory purposes, we speculate that in the context of sulfate-dependent AOM, the observed behavior could reflect the co-occurrence of methane re-cycling, along with methane degradation.

5.3.3. Reversibility of the AOM pathway in the Black Sea sediments?

At the base of the SMTZ, $\Delta^{13}CH_3D$ and $\Delta^{12}CH_2D_2$ values yield apparent temperatures of -14^{+15}_{-14}°C and 26^{+29}_{-24}°C, thus consistent with *in situ* temperatures of *ca.* 10 °C. This may suggest a mechanism for re-equilibrating the methane isotopologues in these sedimentary horizons. Under low sulfate concentrations, it is speculated that methanotrophic Archaea may promote partial reversibility of the AOM reaction, or at least of some of its key enzymatic steps. This would imply that a substantial amount of methane could be re-formed or "re-bonded" during the process (Holler et al., 2011, Yoshinaga et al., 2014; Timmers et al., 2017; Marlow et al., 2014; Beulig et al., 2019; Young, 2019; Wegener et al., 2021). The concept of reversibility during AOM suggests that the isotopic evolution of products and substrates may be partly controlled by equilibrium effects instead of being solely controlled by kinetic effects. From our data, the fact that bottom $\Delta^{13}CH_3D$ and $\Delta^{12}CH_2D_2$ values are close to equilibrium values at *in situ* temperatures argue in favor of such a mechanism.

To explore the potential role of reversibility on methane isotopologue distribution, we adapted our reactive transport model following Burdige et al., (2016) and Chuang et al., (2019) (see Supplementary Material). In this simple model, the degree of

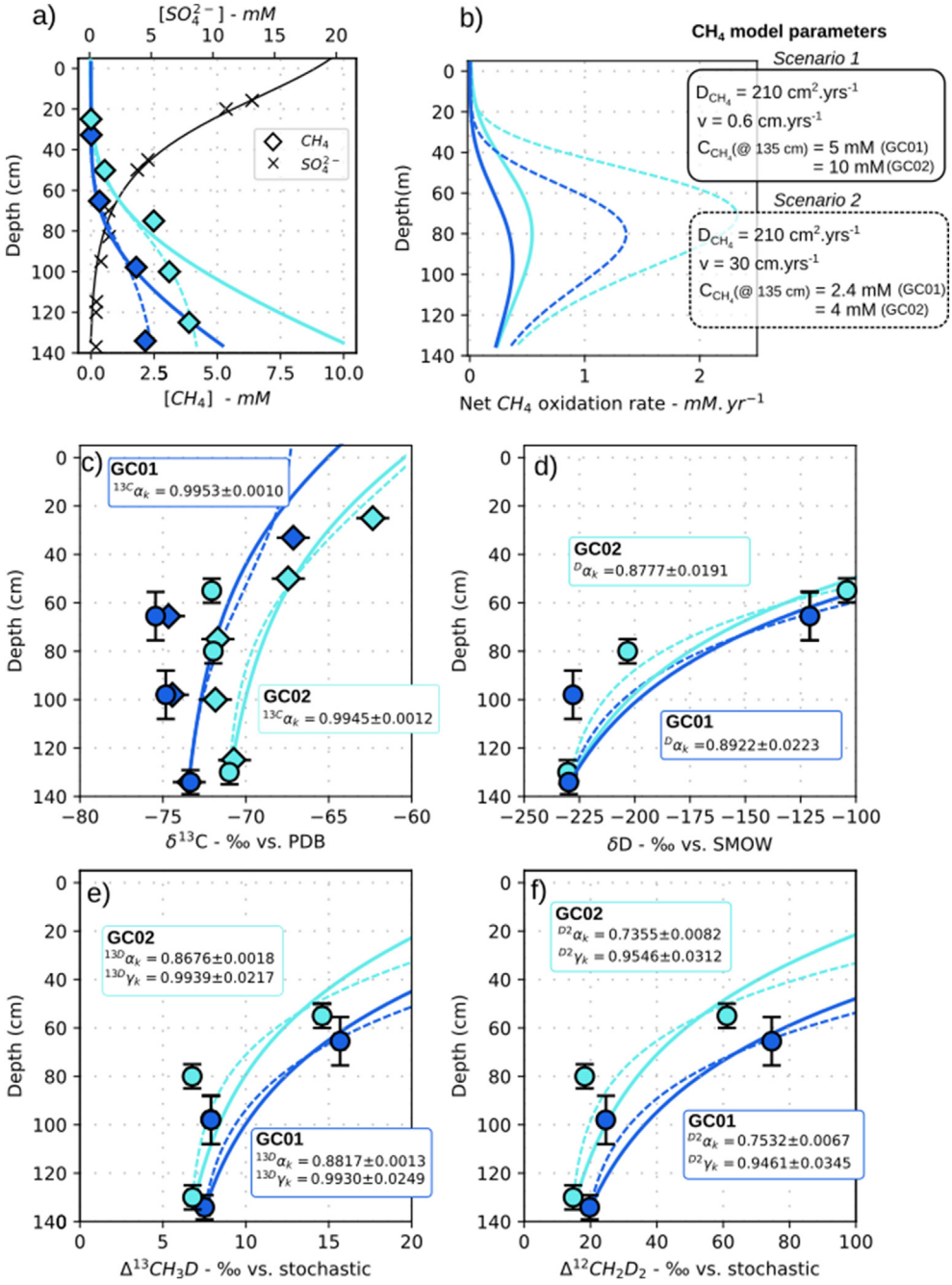

Fig. 7. Inferring apparent isotope fractionation factors of methanotrophy in sediments of the Black Sea. Reactive transport Eq. (7) is solved for methane concentration, and subsequently for each isotopologues. Over this small depth interval (<1.5 m), the effective diffusion coefficient of methane is considered homogeneous and taken as 190 $cm^2 \cdot yr^{-1}$ (*i.e.* diffusion coefficient of methane in water modulated by a tortuosity coefficient). Diffusion is assumed to fractionate methane isotopologues according to their masses, with D_{17}/D_{16} = 0.997 and D_{18}/D_{16} = 0.994 (see discussion in Giunta et al., 2021). To model the CH_4 concentration profiles, two scenarios with distinct boundary conditions and input parameters are considered. In scenario (1), we assume that CH_4 has significantly degassed from the cores prior to sampling. Thus, measured CH_4 concentrations above saturation at ambient conditions are underestimated. The bottom CH_4 bottom concentrations are assumed be at the minimum of 5 mM and 10 mM for GC01 and GC02, respectively. The vertical fluid flow velocity is taken as 0.6 $cm.yr^{-1}$, as inferred at first order from dissolved Cl^- concentrations (Fig. S2). In scenario (2), we assume that the measured CH_4 concentrations accurately capture the *in situ* concentrations (*i.e.* no degassing prior to sampling), thus requiring an substantial vertical flow velocity to fit the data (here set to 30 $cm.yr^{-1}$). The two scenarios have great impact on the oxidation rate profiles (panel b.) but not on the extrapolated fractionation factors (see also Fig S4 and S5). The model suggests that clumped isotope fractionation factors with γ significantly below unity are required to produce the extremely positive $\Delta^{13}CH_3D$ and $\Delta^{12}CH_2D_2$ values measured here.

reversibility r is set to control the extent to which kinetic or equilibrium effects are expressed among methane isotopologues. The reversibility is defined as the ratio between the backward and forward reaction rates, and may range between 0 (irreversible reaction) and 1 (fully reversible reaction). The forward reaction rate corresponds to the methane oxidation rate, and is associated with a kinetic fractionation factor α_F such as derived in the previous sections. The backward reaction rate corresponds to the rate of methane re-forming during the reaction (*i.e.* yielding to a methane back-flux), and is related to the forward rate constant through the equilibrium fractionation factor, such that $\alpha_B = \alpha_F \cdot \alpha_{Eq}$, where α_{Eq} is the equilibrium fractionation factor, generally well known either

from theoretical calculations or from experiments. Several additional assumptions were made for this modeling:

1. At thermodynamic equilibrium (for $r = 1$), it is assumed that the relative distribution of clumped isotopologues must be that of isotope-bond equilibrium at local temperature and that the bulk methane $^{13}C/^{12}C$ and D/H are in isotope equilibrium with DIC or water, respectively;
2. The reversibility of the AOM reaction was parameterized in our model to vary as a step function of a threshold sulfate concentration (following *e.g.* Yoshinaga et al., 2014; Chuang et al., 2019). This threshold concentration was set to 0.55 mM for GC01, corresponding to the sulfate concentration at 98 cm depth. This is where we estimate from observation of δD, $\Delta^{13}CH_3D$ and $\Delta^{12}CH_2D_2$ profiles that the *change* of reversibility must occur. Note this value is consistent with the 0.5 mM threshold sulfate concentration inferred from AOM incubations (Yoshinaga et al., 2014). Thereby, for sulfate concentrations higher than the threshold concentration, the reversibility of AOM was fixed to $r = 0.05$, a minimal reversibility value determined under high sulfate concentrations (Holler et al., 2011). For concentrations below that threshold value, the reversibility was treated as a fitting parameter and left for optimization on the data.
3. Considering the small and shallow depth interval investigated here (<150 cm), we assumed that the isotopic composition of the porewater was homogeneous, with $\delta D_{water} = -15$ ‰ (a typical value for bottom seawater in the Black Sea, Swart, 1991; Dubinin et al., 2014).

With the aforementioned assumptions, our model may solve the reactive transport equations for δD, $\Delta^{13}CH_3D$ and $\Delta^{12}CH_2D_2$ with for each, two parameters left for optimizations: the value of r for sulfate concentrations below 0.55 mM (*i.e.* for depths greater than 98 cm depth), the kinetic fractionation factor of AOM. For modeling bulk $\delta^{13}C$, we assumed a r value similar than that optimized on bulk δD data, and left $\delta^{13}C_{DIC}$ as a free parameter to be optimized on the $\delta^{13}C_{CH4}$ data.

For GC01, the best fits with δD, $\Delta^{13}CH_3D$ and $\Delta^{12}CH_2D_2$ are obtained with, for each profile, a reversibility of the AOM reaction as high as *ca.* 0.98 for sulfate concentrations below 0.55 mM (Fig. 8b and Fig. S4). This suggests that AOM is operating close to thermodynamic equilibrium at the base of the SMTZ, consistent with $\Delta^{13}CH_3D$ and $\Delta^{12}CH_2D_2$ data being close to intra-molecular equilibrium at environmental temperatures. Though preliminary, this conclusion is in line with several recent studies, all suggesting that under low sulfate concentrations, a strong reversibility of the AOM pathway or at least of some of its key intermediate reactions is expected. For instance, incubations of ANME with their sulfate-reducing bacterial partners point to a reversibility of the AOM pathway as high as 0.75 under sulfate concentrations of 0.5 mM (Yoshinaga et al., 2014). Likewise, modeling of the carbon cycle in sediments offshore Taiwan allow estimating a reversibility of the AOM pathway ranging between 0.91 and 0.99 for sulfate concentrations ranging between 5 and 0.05 mM (Chuang et al., 2019). The recent study by Wegener et al., (2021) provided some more nuanced conclusions. In their incubation experiments with only 0.05 mM sulfate, they concluded that the overall reversibility is no more than 0.15. Through sophisticated biochemical modeling of key intermediate reactions of the AOM pathway, they identified some intermediate steps operating close to equilibrium (*i.e. high* reversibility), and some other such as the terminal Formyl-methanofuran dehydrogenase (Fmd)-catalyzed reaction, being essentially controlled by kinetics (*i.e.* non-reversible). As a result on methane isotopic compositions, it is expected that the linear chained-reaction for carbon isotope equilibration between methane and DIC may rarely be achieved, as this would require all intermediate steps to be operating close to equilibrium. By contrast, hydrogen atoms are subtracted from the carbon through a branched reaction at several intermediate steps during the AOM pathway. Thus the high reversibility of the first metabolic step (*i.e.* activation of HS-CoB intermediate by Mcr enzyme) may allow sufficient hydrogen exchange with intra-cellular water to promote the equilibration of the methane δD as well as of the $\Delta^{13}CH_3D$ and $\Delta^{12}CH_2D_2$ (Wegener et al., 2021). Accordingly, it is probably not accurate to model the $\delta^{13}C$ data with the same reversibility value than the one inferred on δD data like we did here. In our model, overestimating the reversibility associated with the carbon isotope exchange would result in overestimating the $\delta^{13}C$ of the DIC. It will not affect the extrapolation of the $^{13}\alpha$ value however. Here we infer $\delta^{13}C_{DIC} = -6$ ‰, a rather *high* value for system presumably controlled by AOM. This may support the idea that the reversibility value (*i.e* of 0.98) applied to carbon isotopes in our model is indeed overestimated. Regardless of the magnitude of the reversibility, our model also suggests that the depth at which the *change* of reversibility occurs may not be the same for carbon and for hydrogen exchanges. From both the model and the data, the δD, $\Delta^{13}CH_3D$ and $\Delta^{12}CH_2D_2$ values start increasing at 65 cm depth, which can be understood as kinetics outpacing equilibrium effects at sulfate concentrations higher than 0.55 mM. Yet at this depth, measured $\delta^{13}C$ are at their minimal value. This observation is compelling as it suggests that the bulk carbon isotopes are still partially controlled by equilibrium at this depth, whereas hydrogen isotopes would be dominantly controlled by kinetics. We note that such apparent "delay" between the $\delta^{13}C$ and δD data seems to occur as well in the few other SMTZ datasets where δD was investigated with $\delta^{13}C$ (Alperin et al., 1988; Martens et al., 1999; Kessler et al., 2006; Egger et al., 2016). For GC01 specifically, a better fit of the model with $\delta^{13}C$ data can be obtained if setting the threshold sulfate concentration to 2.2 mM (Fig. 8a). This observation probably further illustrates the limitation of considering microbial AOM as a single reaction with a unique reversibility profile applying to both carbon and hydrogen isotopes.

Overall, taking into account the reversibility of the AOM reaction persistently results in isotope fractionation of larger magnitude for all isotopologues, with $^{13}\alpha = 0.9928$ (*ca.* 7.2 ‰), $^{D}\alpha = 0.8180$ (*ca.* 182 ‰); $^{13D}\alpha = 0.7942$ and $^{D2}\alpha = 0.6018$. The bulk isotope fractionation factors extrapolated with this revised model appear more consistent with those extrapolated from laboratory incubations (Fig. 6), though the fractionation factor for bulk carbon is again of limited magnitude. An underestimation of the $^{13}\alpha$ may well results from how we simplified the concept of reversibility in our model. Note that setting the threshold sulfate concentration to 2.2 mM for carbon isotope yields slightly higher magnitude of fractionation, with $^{13}\alpha = 0.9911$ (*ca.* 8.9 ‰). As an important result, the intrinsic clumped isotope effects are found to be significantly below unity, with $^{13D}\gamma = 0.9867 \pm 0.0019$ and $^{D2}\gamma = 0.9152 \pm 0.00$ 19. This particular deviation from product of bulk isotope fractionation factors may be crucial in identifying AOM in natural environments. The same modeling can be applied to GC02, yielding to similar results (see Supplementary). Sensitivity analyses performed for several of the input parameters have almost negligible influence on the determination of fractionation factors (see Supplementary), so we suggest our extrapolations are relevant to natural environments where methane degradation is dominated by sulfate-dependent AOM.

5.4. Implications for the identification of the methane bio-signatures

By measuring the resolved abundances of $^{13}CH_3D$ and $^{12}CH_2D_2$, our study identifies fundamental distinctions between two main types of biological degradation pathways, in line with recent

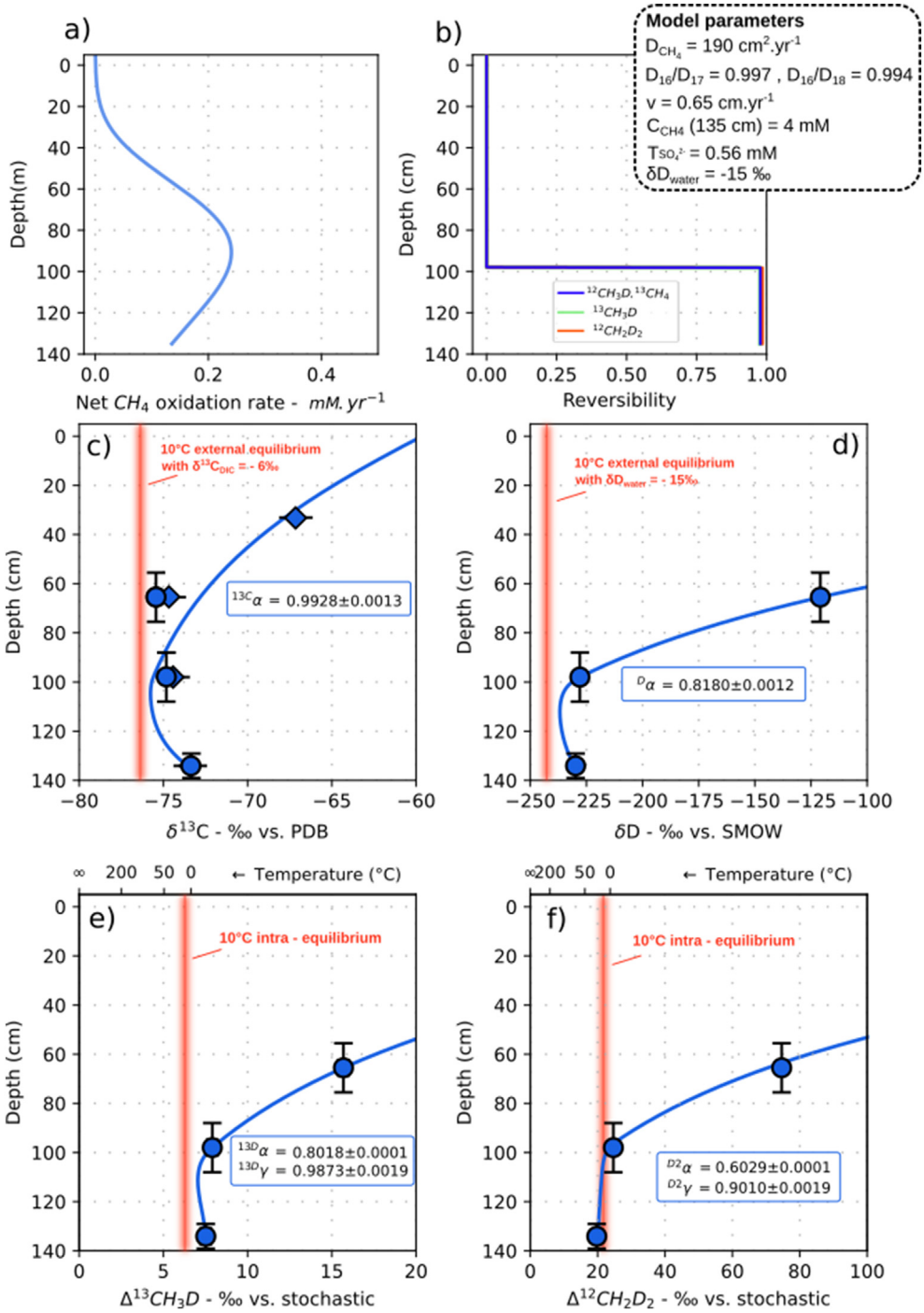

Fig. 8. Reactive transport modeling with partially reversible AOM reaction in the core GC01. The CH_4 concentration profile is modeled according to Scenario 1 (see Fig. 7). In this depth interval, the pore-water is assumed to be isotopically homogeneous with $\delta D_{water} = -15$ ‰. The reversibility of the AOM reaction is set here to depend on a threshold sulfate concentration of 0.55 mM (*ca.* 95 cm depth, panel b.). Below this concentration, the reversibility value is optimized to fit the data and found to be of *ca.* 0.98 (panel b.). Such a high reversibility of the AOM reaction (or at least part of its intermediate reactions) is required to explain why $\Delta^{13}CH_3D$ and $\Delta^{12}CH_2D_2$ are approaching equilibrium at the bottom of the cores, despite net methane degradation presumably occurring (panel a.). Meanwhile, above the threshold sulfate concentration of 0.55 mM, AOM reaction is assumed to be largely dominated by kinetics, with a minimal reversibility of 0.05 (Holler et al., 2011). The kinetic isotope fractionation factors derived here further support the idea that clumped isotopologue fractionation factors of AOM exhibit a significant departure from the product of bulk isotope fractionation factors ($\gamma < 1$). Other scenarios for modeling CH_4 concentration profile in GC01, as well as in GC02, result in similar fractionation factors and maximum reversibility values ranging between 0.72 and 0.98 (Fig. S4 and S5).

laboratory studies on $^{13}CH_3D$ (Wang et al., 2016; Ono et al., 2021). Our data suggest that in nature, AeOM likely occurs with negligible intrinsic 'clumped' isotope effect. This means that the isotope fractionation factors associated to the degradation of rare methane isotopologues is expected to be close to the product of bulk isotope fractionation factors ($\gamma \approx 1$). By contrast, sulfate-dependent AOM appears to be associated with significant clumped isotope effects, with fractionation factors for $^{13}CH_3D$ and $^{12}CH_2D_2$ being significantly lower than product of bulk isotope fractionation factors ($\gamma < 1$). This can produce extremely positive $\Delta^{13}CH_3D$ and

$\Delta^{12}CH_2D_2$ values, as high as 16 and 75 ‰, respectively. The fundamental mechanism for explaining this difference between the two pathways is currently unknown, but may reflect different geometry of transition states between the enzyme involved in AeOM (soluble methane monooxygenase, sMMO) and enzyme involved in AOM (methyl coenzyme M reductase, Mcr)(Ono et al., 2021).

Our study demonstrates that above a certain sulfate concentration, the AOM reaction does overprint strong kinetic effects on residual methane isotopologues, including $^{13}CH_3D$ and $^{12}CH_2D_2$. The observation is consistent with laboratory studies (Ono et al., 2021), but at odd with postulates that in nature AOM would mostly promote equilibration of clumped isotopologues, even at high sulfate concentrations. In sediments of the Baltic Sea, Ash et al., (2019) observed a slight increase of $\Delta^{13}CH_3D$ and $\Delta^{12}CH_2D_2$ values along with decreasing of CH_4 concentrations in sediments of the Baltic Sea. This observation is *per se* consistent with the expression kinetic isotope effects as observed in our data from the Black Sea sediments. Yet, because the sample with the lowest concentration measured in the Baltic Sea sediments was plotting on the equilibrium curve, the authors interpreted the $\Delta^{13}CH_3D$ and $\Delta^{12}CH_2D_2$ profiles as reflecting a progressive re-equilibration of the methane alongside to net methane degradation (Ash et al., 2019). Another possibility is that this sample-set from the Baltic Sea was not covering a range of methane concentration large enough to observe to full expression of kinetic effects among $\Delta^{13}CH_3D$ and $\Delta^{12}CH_2D_2$, and perhaps that the sample measured with the lowest concentration (only ~50 % of maximum measured concentration) was only coincidentally plotting on the equilibrium line. Accordingly, one could suspect that in the Baltic Sea sediments, samples with even lower CH_4 concentrations (*i.e.* more degraded) would show the more positive values indicative of kinetic fractionation. Note that in our modeling effort of the Black Sea sediment methane, we do suggest that AOM could promote equilibration of methane isotopologues (as a result of higher reversibility of the reaction), but only in low sulfate concentrations zones. Thus, although net methane oxidation may be occurring in these low-sulfate horizons, it can be speculated that overall, most of methane loss through AOM would be associated to kinetic isotope effects and result in large positive excursions of both $\Delta^{13}CH_3D$ and $\Delta^{12}CH_2D_2$.

5.4.1. Closed-system versus open-system methanotrophy

The manner in which a 'primary' $\Delta^{13}CH_3D$-$\Delta^{12}CH_2D_2$ signature of a methane may be modified by a secondary process such as methanotrophy depends crucially on the magnitude of clumped isotope fractionation factors ($^{13D}\alpha$ or $^{D2}\alpha$), and their deviations from the product of bulk isotope fractionation factors ($^{13D}\gamma$ and $^{D2}\gamma$). Another fundamental aspect is whether the system in which the methanotrophy takes place is considered to be closed or open (Wang et al., 2016; Haghnegahdar et al., 2017; Ono et al., 2021). In a closed system, the methane reservoir is being degraded without being replenished. The evolution of a given isotopic ratio may be described by the classic Rayleigh equation $R = R_{ini} \cdot f^{\alpha-1}$, where R_{ini} is the initial isotopic ratio and f is the remaining fraction of methane. After some simplifications, the evolution of $\Delta^{13}CH_3D$ and $\Delta^{12}CH_2D_2$ may simply be described as (Wang et al., 2016):

$$\Delta^{13}CH_3D = \Delta^{13}CH_3D_{ini} + \ln(f) \cdot (^{13D}\gamma \cdot {}^{13}\alpha \cdot {}^{D}\alpha - {}^{13}\alpha - {}^{D}\alpha + 1) \quad (12)$$

and

$$\Delta^{12}CH_2D_2 = \Delta^{12}CH_2D_{2\,ini} + \ln(f) \cdot (^{D2}\gamma \cdot {}^{D}\alpha^2 - 2^{D}\alpha + 1) \quad (13)$$

These simple formulations show that, depending on the γ value, $\Delta^{13}CH_3D$ and $\Delta^{12}CH_2D_2$ may either way evolve towards more negative or more positive values for a methanotrophic reaction occurring in a closed system. The threshold conditions are met for $^{13D}\gamma = (^{13}\alpha + {}^{D}\alpha - 1)/(^{13}\alpha \cdot {}^{D}\alpha)$ and $^{D2}\gamma = (2 \cdot {}^{D}\alpha - 1)/{}^{D}\alpha^2$. Accordingly, for any γ values sufficiently closed to unity such as the AeOM reaction, $\Delta^{13}CH_3D$ and $\Delta^{12}CH_2D_2$ are predicted to evolve towards more *negative* compositions (Fig. 9). By contrast, the $^{13D}\gamma$ and $^{D2}\gamma$ values of 0.9867 and 0.9152 determined in this study for AOM are both below unity and most importantly, below threshold conditions (calculated here of 0.9984 and 0.9504, respectively). Thus, AOM reaction in closed system should promote evolution towards more *positive* values of the residual methane (Fig. 9). Abiotic oxidation of methane with •OH or •Cl, the two main methane sinks in the atmosphere, were predicted through *ab initio* calculations to result in $^{13D}\gamma$ and $^{D2}\gamma$ values similar to those determined for AOM (Whitehill et al., 2017; Haghnegahdar et al., 2017). However, given the $^{13}\alpha$ and $^{D}\alpha$ values associated with these abiotic reactions (*i.e.* of greater magnitude than for AOM), γ values are above the threshold conditions yielding to $\Delta^{13}CH_3D$ and $\Delta^{12}CH_2D_2$ decreases for these two processes. As a consequence, this leaves AOM the sole methane oxidation process identified so far to promote $\Delta^{13}CH_3D$ and $\Delta^{12}CH_2D_2$ enrichments of the residual methane.

In the case of an open system however, these perspectives may change radically. In a reservoir where a source of methane persists alongside to methanotrophy as a sole sink of methane, the basic mass balance equation applies: $dn_i/dt = S_i - k_i n_i$, where n_i is the moles of isotopologue i in the system, S_i its source term and k_i its oxidation rate. At steady-state ($dn_i/dt = 0$), the clumped isotopo-

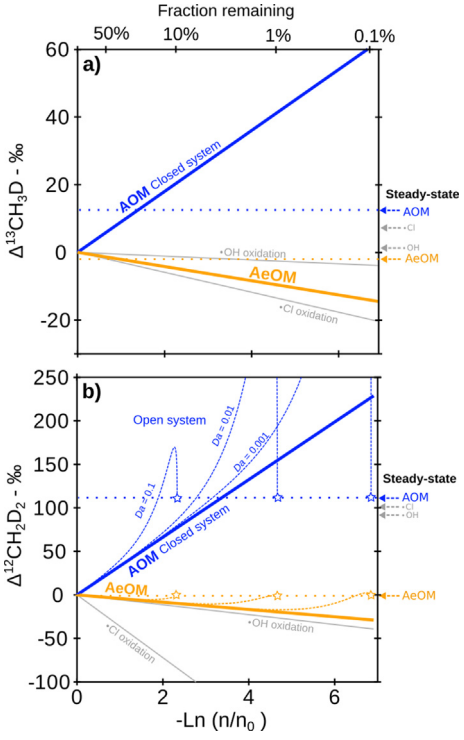

Fig. 9. Behaviors of (a.) $\Delta^{13}CH_3D$ and (b.) $\Delta^{12}CH_2D_2$ during methanotrophy in a closed or in an open system as function of remaining fraction of methane n/n_0, with n_0 being the initial quantity of methane in the reservoir. Isotope fractionations factors used for these plots are from this study for AOM (GC01, Fig. 8) and AeOM (Lake Pavin water column, Fig. 5), and from Haghnegahdar et al., (2017) for •Cl and •OH oxidation reactions. In a closed system, the evolution isotopologues abundances is described with a simple Rayleigh formalism, and simplifies for clumped isotopologues in Eqs. (12) and (13). In an open system, each isotopologue satisfies the basic mass balance equation $dn/dt = S - kn$. The solution can be written in the form $n(t)/n_0 = e^{-kt} + Da(1 - e^{-kt})$, where Da is the Damköhler number establishing the relevance of the reaction over that of the source such that $Da = \tau_k/\tau_S$, with $\tau_k = 1/k$ and $\tau_S = n_0/S$. Eventually, all open systems converge to unique steady-state signatures (doted-lines in panels a. and b.) that can be approached with Eqs. (14) and (15), but are expected to mimic closed system behavior for sufficiently small Da values ($\ll$1, dashed-line in panel b.).

logue compositions may be simply derived in the form of (Whitehill et al., 2017; Haghnegahdar et al., 2017):

$$\Delta^{13}CH_3D = \Delta^{13}CH_3D_{source} - \ln(^{13D}\gamma) \quad (14)$$

and

$$\Delta^{12}CH_2D_2 = \Delta^{12}CH_2D_{2source} - \ln(^{D2}\gamma) \quad (15)$$

Thus, the $\Delta^{13}CH_3D$ and $\Delta^{12}CH_2D_2$ steady-state signatures in an open system do not depend on bulk isotope fractionation factors. Accordingly, for a system dominated by AeOM, the clumped signatures are expected to remain relatively closed to the source signature (because $\gamma \approx 1$), whereas in a system dominated by AOM, they should be more positive (because $\gamma < 1$) by *ca.* 13 and 105 ‰, respectively. Note that in the case of •OH or •Cl oxidation reactions, the steady-state signatures are also expected to be more positive than the source signatures, especially for $\Delta^{12}CH_2D_2$, where the offset would be in the vicinity of +105 ‰ (similar to that of AOM, see Fig. 9b).

One may expect that in nature, open systems are prevailing, with methane sources and sinks eventually reaching a steady-state. In the atmosphere for instance, where oxidation with •OH radicals is considered the dominant methane sink, the $\Delta^{12}CH_2D_2$ is predicted to be essentially reflecting a steady-state signal with values has high as *ca.* 130 ‰ (Haghnegahdar et al., 2017), thus contrasting with more *negative* values one would see for oxidation of methane in a closed system. Arguably, lake or sediments (pore-) water columns, such as investigated here, may also be considered as open systems since both production and degradation of methane are co-occurring. Note however that for systems where the characteristic time of the reaction (τ_k) is much smaller than the characteristic time of the source flux (τ_S), the 'trajectory' of the isotopic values towards steady-state in fact closely mimics that of a closed-system (Fig. 9b). One may use the non-dimensional Damköhler number ($Da = \tau_k/\tau_S$) to evaluate the relevance of the reaction over that of transport. In a system where transport is dominated by diffusion, Da is best approximated by $D/(k \cdot L^2)$, where D is the diffusion coefficient and L is the length of the system. Therefore, at the scale of geological systems such as those investigated here, we may generally expect $Da \ll 1$ (*e.g.* Bhatnagar et al., 2008). Accordingly, in a lake or sediment undergoing methanotrophic reaction, the residual methane flux towards the atmosphere (or the open sea water) may well be that of an open system steady-state, but the "path" towards these signatures may essentially exhibit those of a closed-system.

5.4.2. The 'grayness' of microbial methane isotopic fingerprints

Being able to identify the biological production and degradation routes of methane is a major challenge for a broad range of disciplines, including atmospheric chemistry, oil and gas exploration, oceanography, and agriculture. This will likely represent a corner-stone for the search for life in our solar system (*e.g.* Oehler and Etiope, 2017; House et al., 2022). To this end, the methane bulk isotope geochemistry ($\delta^{13}C$ and δD) is widely used, but the interpretation of these signatures is largely dependent on the assumptions made regarding carbon and hydrogen precursors and their isotopic compositions, on the associated fractionation factors, and on the evaluation of (potentially multiple) secondary processes that may have impacted the methane. The present study further supports the idea that the use of methane clumped isotopologues may be useful in identifying methane bio-signatures and related metabolisms, though they may rarely provide a "silver bullet" of a microbial activity.

In nature, we may simply distinguish two types of methane samples. Those with $\Delta^{13}CH_3D$ and $\Delta^{12}CH_2D_2$ signatures indicative of equilibrium, and those which are not at equilibrium (Fig. 10). Regardless of the apparent equivalent temperature of a sample, it is still unclear whether equilibrium signatures are obtained during formation of the methane (thus reflecting actual formation temperature), or whether they are acquired after (thus potentially reflecting another temperature experienced by the methane) (Stolper et al., 2017). Recent studies have advocated for post-formation *equilibration* or *re-equilibration* of the methane isotopologues in hydrothermal systems or sedimentary reservoirs seeping at the seafloor (Labidi et al., 2020; Giunta et al., 2021; Beaudry et al., 2021). The exact mechanisms involved for such isotope equilibration are unclear but are speculated to be promoted by surface-catalyzed exchange onto clay or metal minerals. Importantly, these 'abiotic' mechanisms seem to be restricted to temperatures >90 °C. Thus, it is reasonable to suggest that a low temperature equilibrium signal in a natural sample is, to some extent, as simple criteria to support a biological mediation of the methane. The mechanism by which microbial methane acquires a low temperature equilibrium signal is debated as well and could result from slow rate of methanogenesis (*e.g.* Wang et al., 2015), or from methane re-cycling and *equilibration* by organisms involved in AOM (*e.g.* Young et al., 2017). In this paper, we suggest that near equilibrium signatures at the base of the SMTZ in the Black Sea are promoted by AOM reaction occurring with a high degree of reversibility due to low sulfate content. This raises the possibility that such reversibility may persist even deeper in the sediment including in 'methanogenesis horizons'. Regardless of the mechanism (*slow* methanogenesis or AOM re-cycling), low temperature equilibrium signatures point towards a microbial mediation of methane.

Alternatively, it is clear that a methane sample exhibiting $\Delta^{13}CH_3D$ and $\Delta^{12}CH_2D_2$ disequilibrium signatures could also reflect a microbial activity. Laboratory culture of methanogens have persistently result in large disequilibrium signatures, often characterized by negative $\Delta^{12}CH_2D_2$ values. These signatures are recognized in certain ecosystems where microbial methanogenesis is the only plausible production route, whether in swamps, rumen or in lake water columns such as in the present study. Yet, it is now established that disequilibrium signatures are not exclusive to microbial production routes. Both laboratory and computational works now suggest that similar signatures can be obtained during early stages of thermocatalytic cracking of organic matter (*e.g.* Xia and Gao, 2019; Dong et al., 2021). Likewise, low temperature abiotic generation (<90 °C) through Sabatier-type reactions may also produce similar disequilibrium (Young et al., 2017; Cao et al., 2019). These different formation pathways have in common the fact that hydrogen atoms with disparate D/H ratios can contribute to the assembly of the product CH_4 molecules (*e.g.*, Taenzer et al. 2020). Taken together, these compelling observations suggest that in fact, most methane production routes may be associated with significant disequilibrium among clumped isotopologues. Generally, this prevents one from using clumped isotopologue disequilibrium as a fingerprint for microbial activity, although the combination of both negative $\Delta^{13}CH_3D$ and ΔCH_2D_2 seems to be a good indicator of microbial methanogenesis. Furthermore, our study further demonstrates that secondary processes such as methanotrophic reactions could contribute to disequilibrium. To the degree the system is closed, the kinetic isotope effects associated with AeOM will produce negative $\Delta^{13}CH_3D$ and $\Delta^{12}CH_2D_2$ offsets, and may thus generate disequilibrium or even "enhance" a pristine disequilibrium signature inherited from the methane's formation. Microbial AOM is also associated with kinetic isotopes effects that will contribute to produce disequilibrium through positive enrichments in $\Delta^{13}CH_3D$ and $\Delta^{12}CH_2D_2$. We suggest that extreme positive $\Delta^{13}CH_3D$ and $\Delta^{12}CH_2D_2$ values may be a strong argument for microbial activity, as AOM is to date the sole identified mechanism capable of producing such positives values. Such behavior may in future, constitute a target for life detection on

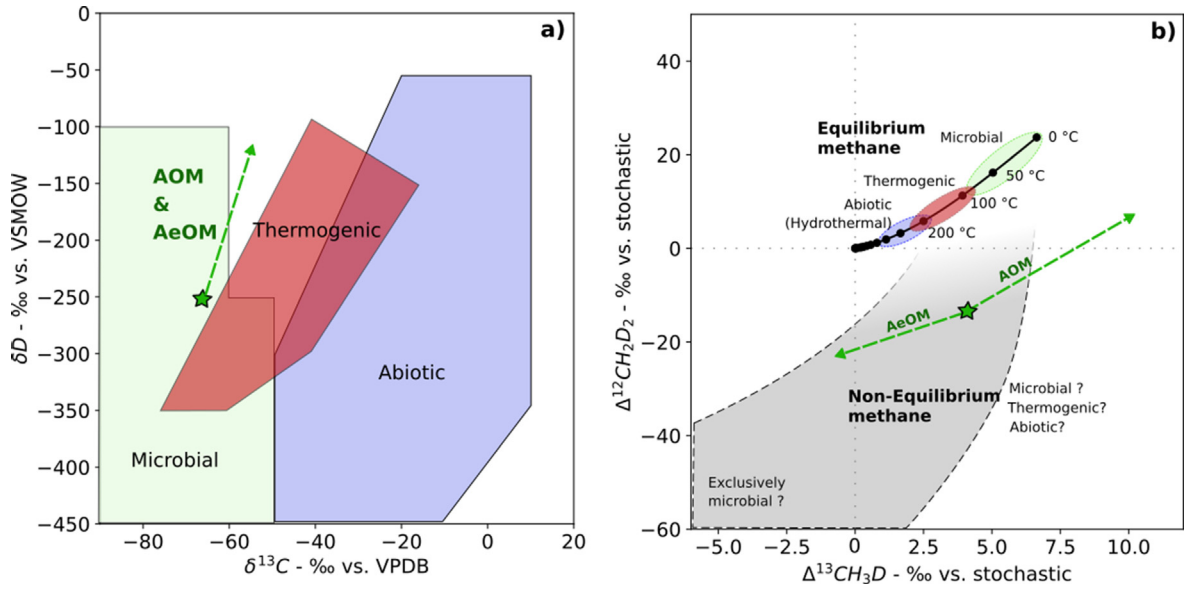

Fig. 10. Biological and non-biological processes in the bulk isotope space (a) and the clumped isotope space (b). Empirical fields for microbial, thermogenic and abiotic attribution based on δ13C and δD are those reported in Milkov and Etiope (2018). In the clumped isotope space, we may distinguish natural methane samples with equilibrium or non-equilibrium signatures. To date, it was recognized that abiotic methane from marine hydrothermal vents, thermogenic methane in sedimentary reservoirs or microbial methane in the deep biosphere are likely to be plotting on or closed to the equilibrium curve (Young et al., 2017, 2019; Giunta et al., 2019; Ash et al., 2019; Labidi et al., 2020; Zhang et al., 2021; Mangenot et al., 2021). Thus, for natural methane samples with equilibrium signatures, the apparent low temperature is perhaps a simple criteria to support a biological mediation of the methane. Note that there is a range of equivalent temperatures (*ca.* 80–120 °C) that would encompass both microbial and thermogenic methanogenesis temperature ranges, so that the apparent temperature may not always be relevant for discriminating between these two processes. On the other hand, methane with non-equilibrium signatures (gray) are thought to reflect kinetic and or statistical effects associated with the methane synthesis (*e.g.* Taenzer et al., 2020). It is now established from field, experimental and computational studies that all methane production pathways, whether abiotic, thermogenic or microbial, can produce disequilibrium signatures among methane isotopologue (*e.g.* Wang et al., 2015; Young et al., 2017; Gruen et al., 2018; Cao et al., 2019; Dong et al., 2021). Thus, a disequilibrium signature may not be sufficient to infer a biological mediation (although both negative $\Delta^{13}CH_3D$ and $\Delta^{12}CH_2D_2$ signatures seem to be exclusive to microbial methanogenesis so far). Secondary processes such methanotrophic reactions will affect pristine source signature of the methane and may further contribute to, or generate, disequilibrium among clumped isotopologues. Here, we report in both spaces the general trajectory of methane undergoing microbial oxidation through AOM or AeOM.

other planetary bodies such as Mars or Titan, where AOM is considered to be a thermodynamically viable metabolism for putative organisms (Norman, 2011; Marlow et al., 2014; House et al., 2022).

6. Conclusion

We investigated two natural settings where microbial methanotrophy degraded nearly quantitatively methane being produced by microbial methanogenesis. In the Lake Pavin, where the methanotrophy is dominated by AeOM, the bulk $\delta^{13}C$ and δD values of the residual methane are increasing alongside to methanotrophy, whereas $\Delta^{13}CH_3D$ and $\Delta^{12}CH_2D_2$ values are decreasing. By using a simple 1-D reactive transport model, we extrapolated apparent fractionation factors that are at the low-end but consistent with the literature, with $^{13}\alpha$ = 0.9978, $^{D}\alpha$ = 0.9610, $^{13D}\alpha$ = 0.9608 and $^{D2}\alpha$ = 0.9261. Importantly, fractionation factors for clumped isotopologues inferred from our model are similar to the product of bulk isotope fractionation factors. In the Black Sea sediments, where methanotrophy is dominated by sulfate-AOM, the bulk $\delta^{13}C$ and δD values of the residual methane are increasing alongside to methanotrophy as per in the Lake Pavin, but $\Delta^{13}CH_3D$ and $\Delta^{12}CH_2D_2$ values are instead showing extreme positive enrichments, up to 15.7 and 74.6 ‰, respectively. These values are the most positive values reported so far, and must result from fractionation factors for clumped isotopologues that significantly deviate from the product of bulk isotope fractionation factors. These contrasting behaviors between a system dominated by AeOM and a system dominated by AOM illustrate the fundamental distinction between the two types of metabolisms. We suggest the data presented here, together with the fractionation factors extrapolated from simple reactive transport modeling, may help to further identify and constrain these processes, both of them constituting major methane sinks in the global methane budget on Earth.

Data availability

Data will be made available on request.

Declaration of Competing Interest

The authors declare that they have no known competing financial interests or personal relationships that could have appeared to influence the work reported in this paper.

Acknowledgments

We thank the captain, his crew, V. Radulescu and S. Balan from GeoEcoMar and the scientific team on-board the R/V Mare Nigrum. We thank A-S. Alix for providing the bathymetric maps and V. Guyader for support on ionic chromatography. We thank A. Roman and T. Kremer for support on developing the reactive transport model. We also thank L. Toffin, E. Viollier, A. Lehours for constructive discussions. Lastly, we thank Ed Hornibrook (AE), together with David T. Wang and two anonymous reviewers for comments that improved this manuscript. This work was supported by ISblue project, Interdisciplinary graduate school for the blue planet (ANR-17-EURE-0015) and co-funded by a grant from the French government under the program "Investissements d'Avenir". The study also received funding from the ENVRI-PlusH2020 project (call 597 Environment, project number 654182).

Appendix A. Supplementary material

Supplementary material to this article can be found online at https://doi.org/10.1016/j.gca.2022.09.034.

References

Aeschbach-Hertig, W., Hofer, M., Schmid, M., Kipfer, R., Imboden, D.M., 2002. The physical structure and dynamics of a deep, meromictic crater lake (Lac Pavin, France). Hydrobiologia 487 (1), 111–136.

Alperin, M.J., Reeburgh, W.S., Whiticar, M.J., 1988. Carbon and hydrogen isotope fractionation resulting from anaerobic methane oxidation. Global Biogeochem. Cycles 2 (3), 279–288.

Andrén, T., Jørgensen, B.B., Cotterill, C., Green, S., 2015. IODP expedition 347: Baltic Sea basin paleoenvironment and biosphere. Sci. Drill. 20, 1–12.

Ash, J., Egger, M., Treude, T., Kohl, I., Cragg, B., Parkes, R.J., Slomp, C., Sherwood Lollar, B., Young, E.D., 2019. Exchange catalysis during anaerobic methanotrophy revealed by 12CH2D2 and 13CH3D in methane. Geochem. Perspect. Lett. 10, 26–30.

Assayag, N., Jézéquel, D., Ader, M., Viollier, E., Michard, G., Prévot, F., Agrinier, P., 2008. Hydrological budget, carbon sources and biogeochemical processes in Lac Pavin (France): constraints from δ18O of water and δ13C of dissolved inorganic carbon. App. Geochem. 23 (10), 2800–2816.

Barnes, R.O., Goldberg, E.D., 1976. Methane production and consumption in anoxic marine sediments. Geology 4 (5), 297–300.

Beal, E.J., House, C.H., Orphan, V.J., 2009. Manganese-and iron-dependent marine methane oxidation. Science 325 (5937). 184–187.1.

Beaudry, P., Stefánsson, A., Fiebig, J., Rhim, J.H., Ono, S., 2021. High temperature generation and equilibration of methane in terrestrial geothermal systems: evidence from clumped isotopologues. Geochim. Cosmochim. Acta 309, 209–234.

Bernard, B.B., Brooks, J.M., Sackett, W.M., 1976. Natural gas seepage in the Gulf of Mexico. Earth Planet. Sci. Lett. 31 (1), 48–54.

Beulig, F., Røy, H., McGlynn, S.E., Jørgensen, B.B., 2019. Cryptic CH 4 cycling in the sulfate–methane transition of marine sediments apparently mediated by ANME-1 archaea. ISME J. 13 (2), 250–262.

Bhatnagar, G., Chapman, W.G., Dickens, G.R., Dugan, B., Hirasaki, G.J., 2008. Sulfate-methane transition as a proxy for average methane hydrate saturation in marine sediments. Geophys. Res. Lett. 35 (3).

Biderre-Petit, C., Jézéquel, D., Dugat-Bony, E., Lopes, F., Kuever, J., Borrel, G., Viollier, E., Fonty, G., Peyret, P., 2011. Identification of microbial communities involved in the methane cycle of a freshwater meromictic lake. FEMS Microbiol. Ecol. 77 (3), 533–545.

Bigeleisen, J., 1955. Statistical mechanics of isotopic systems with small quantum corrections. I. General considerations and the rule of the geometric mean. J. Chem. Phys. 23 (12), 2264–2267.

Boetius, A., Ravenschlag, K., Schubert, C.J., Rickert, D., Widdel, F., Gieseke, A., Amann, R., Jorgensen, B.B., Witte, U., Pfannkuche, O., 2000. A marine microbial consortium apparently mediating anaerobic oxidation of methane. Nature 407 (6804), 623–626.

Borrel, G., Lehours, A.C., Crouzet, O., Jézéquel, D., Rockne, K., Kulczak, A., Duffaud, E., Joblin, K., Fonty, G., 2012. Stratification of Archaea in the deep sediments of a freshwater meromictic lake: vertical shift from methanogenic to uncultured archaeal lineages. PLoS ONE 7 (8), e43346.

Boudreau, B.P., 1997. Diagenetic models and their implementation, Vol. 505. Springer, Berlin.

Brandily, C., LeCuff, N., Donval, J.P., Guyader, V., De Prunele, A., Cathalot, C., Croguennec, C., Caprais, J., Ruffine, L., 2021. A GC-SSIM-CRDS system: Coupling a gas chromatograph with a Cavity Ring-Down Spectrometer for onboard Twofold analysis of molecular and isotopic compositions of natural gases during ocean-going research expeditions. Anal. Chim. Acta 1184, 339040.

Burdige, D.J., Komada, T., Magen, C., Chanton, J.P., 2016. Methane dynamics in Santa Barbara Basin (USA) sediments as examined with a reaction-transport model. J. Mar. Res. 74 (6), 277–313.

Cai, C., Leu, A.O., Xie, G.J., Guo, J., Feng, Y., Zhao, J.X., Tyson, G.W., Yuan, Z., Hu, S., 2018. A methanotrophic archaeon couples anaerobic oxidation of methane to Fe (III) reduction. ISME J. 12 (8), 1929–1939.

Cao, X., Bao, H., Peng, Y., 2019. A kinetic model for isotopologue signatures of methane generated by biotic and abiotic CO2 methanation. Geochim. Cosmochim. Acta 249, 59–75.

Chapron, E., Albéric, P., Jézéquel, D., Versteeg, W., Bourdier, J.L., Sitbon, J., 2010. Multidisciplinary characterisation of sedimentary processes in a recent maar lake (Lake Pavin, French Massif Central) and implication for natural hazards. Nat. Hazards Earth Syst. Sci. 10 (9), 1815–1827.

Chassiot, L., Miras, Y., Chapron, E., Develle, A.L., Arnaud, F., Motelica-Heino, M., Di Giovanni, C., 2018. A 7000-year environmental history and soil erosion record inferred from the deep sediments of Lake Pavin (Massif Central, France). Palaeogeogr. Palaeoclimatol. Palaeoecol. 497, 218–233.

Chowdhury, T.R., Dick, R.P., 2013. Ecology of aerobic methanotrophs in controlling methane fluxes from wetlands. Appl. Soil Ecol. 65, 8–22.

Chuang, P.C., Yang, T.F., Wallmann, K., Matsumoto, R., Hu, C.Y., Chen, H.W., Lin, S., Sun, C., Li, H., Wang, Y., Dale, A.W., 2019. Carbon isotope exchange during anaerobic oxidation of methane (AOM) in sediments of the northeastern South China Sea. Geochim. Cosmochim. Acta 246, 138–155.

Ciccarelli, F.D., Doerks, T., Von Mering, C., Creevey, C.J., Snel, B., Bork, P., 2006. Toward automatic reconstruction of a highly resolved tree of life. Science 311 (5765), 1283–1287.

Coleman, D.D., Risatti, J.B., Schoell, M., 1981. Fractionation of carbon and hydrogen isotopes by methane-oxidizing bacteria. Geochim. Cosmochim. Acta 45 (7), 1033–1037.

Dong, G., Xie, H., Formolo, M., Lawson, M., Sessions, A., Eiler, J., 2021. Clumped isotope effects of thermogenic methane formation: Insights from pyrolysis of hydrocarbons. Geochim. Cosmochim. Acta 303, 159–183.

Douglas, P.M., Gonzalez Moguel, R., Walter Anthony, K.M., Wik, M., Crill, P.M., Dawson, K.S., Smith, D.A., Yanay, E., Lloyd, M.K., Stolper, D.A., Eiler, J.M., Sessions, A.L., 2020. Clumped isotopes link older carbon substrates with slower rates of methanogenesis in northern lakes. Geophys. Res. Lett. e2019GL086756.

Douglas, P.M.J., Stolper, D.A., Smith, D.A., Anthony, K.W., Paull, C.K., Dallimore, S., Wik, M., Crill, P.M., Winterdahl, M., Eiler, J.M., Sessions, A.L., 2016. Diverse origins of Arctic and Subarctic methane point source emissions identified with multiply-substituted isotopologues. Geochim. Cosmochim. Acta 188, 163–188.

Dubinin, A.V., Dubinina, E.O., Demidova, T.P., Kokryatskaya, N.M., Rimskaya-Korsakova, M.N., Kosova, S.A., Yakushev, E.V., 2014. Stable isotope evidence for the Bottom Convective Layer homogeneity in the Black Sea. Geochem. Trans. 15 (1), 1–16.

Egger, M., Kraal, P., Jilbert, T., Sulu-Gambari, F., Sapart, C.J., Röckmann, T., Slomp, C. P., 2016. Anaerobic oxidation of methane alters sediment records of sulfur, iron and phosphorus in the Black Sea. Biogeosciences.

Egger, M., Hagens, M., Sapart, C.J., Dijkstra, N., van Helmond, N.A., Mogollón, J.M., Petersen-Risgaard, N., van der Veen, C., Kasten, S., Riedinger, N., Böttcher, M.E., Röckmann, T., Jorgensen, B.B., Slomp, C.P., 2017. Iron oxide reduction in methane-rich deep Baltic Sea sediments. Geochim. Cosmochim. Acta 207, 256–276.

Eldridge, D.L., Korol, R., Lloyd, M.K., Turner, A.C., Webb, M.A., Miller, T.F., Stolper, D., 2019. Comparison of Experimental vs. Theoretical Abundances of 13CH3D and 12CH2D2 for Isotopically Equilibrated Systems From 1–500◦ C. ACS Earth Space Chem.

Eller, G., Känel, L., Krüger, M., 2005. Cooccurrence of aerobic and anaerobic methane oxidation in the water column of Lake Plußsee. Appl. Environ. Microbiol. 71 (12), 8925–8928.

Etiope, G., 2017. Methane origin in the Samail Ophiolite: comment on "Modern water/rock reactions in Oman hyperalkaline peridotite aquifers and implications for microbial habitability. Geochim. Cosmochim. Acta. Geochim. Cosmochim. Acta 179 (2016), 217–241.

Feisthauer, S., Vogt, C., Modrzynski, J., Szlenkier, M., Krüger, M., Siegert, M., Richnow, H.H., 2011. Different types of methane monooxygenases produce similar carbon and hydrogen isotope fractionation patterns during methane oxidation. Geochim. Cosmochim. Acta 75 (5), 1173–1184.

Gal, F., Gadalia, A., Millot, R., 2015. Geochemical study of a Crater lake: Lake Pavin, France: a view through Li-OH isotopes. Procedia Earth Planet. Sci. 13, 189–193.

Giunta, T., Young, E.D., Warr, O., Kohl, I., Ash, J.L., Martini, A., Mundle, O.C., Rumble, D.R., Pérez-Rodriguez, I., Wasley, M., LaRowe, D.E., Gilbert, A., Sherwood Lollar, B., 2019. Methane sources and sinks in continental sedimentary systems: New insights from paired clumped isotopologues $^{13}CH_3D$ and $^{12}CH_2D_2$. Geochim. Cosmochim. Acta 245, 327–351.

Giunta, T., Labidi, J., Kohl, I.E., Ruffine, L., Donval, J.P., Géli, L., Cagatay, M.N., Lu, H., Young, E.D., 2021. Evidence for methane isotopic bond re-ordering in gas reservoirs sourcing cold seeps from the Sea of Marmara. Earth Planet. Sci. Lett. 553, 116619.

Gonzalez, Y., Nelson, D.D., Shorter, J.H., McManus, J.B., Dyroff, C., Formolo, M., Wang, D.T., Western, C.M., Ono, S., 2019. Precise measurements of $^{12}CH_2D_2$ by tunable infrared laser direct absorption spectroscopy. Anal. Chem. 91 (23), 14967–14974.

Grilli, R., Birot, D., Schumacher, M., Paris, J.D., Blouzon, C., Donval, J.P., Guyader, V., Leau, H., Giunta, T., Delmotte, M., Radulescu, V., Sorin, B., Greinert, J., Ruffine, L., 2021. Inter-Comparison of the Spatial Distribution of Methane in the Water Column From Seafloor Emissions at Two Sites in the Western Black Sea Using a Multi-Technique Approach. Front. Earth Sci. 9 (626372).

Gropp, J., Jin, Q., Halevy, I., 2022. Controls on the isotopic composition of microbial methane. Sci. Adv. 8 (14), eabm5713.

Gruen, D.S., Wang, D.T., Könneke, M., Topçuoğlu, B.D., Stewart, L.C., Goldhammer, T., Holden, J.H., Hinrichs, K.U., Ono, S., 2018. Experimental investigation on the controls of clumped isotopologue and hydrogen isotope ratios in microbial methane. Geochim. Cosmochim. Acta 237, 339–356.

Haghnegahdar, M.A., Schauble, E.A., Young, E.D., 2017. A model for 12CH2D2 and 13CH3D as complementary tracers for the budget of atmospheric CH4. Global Biogeochem. Cycles 31 (9), 1387–1407.

Hallam, S.J., Putnam, N., Preston, C.M., Detter, J.C., Rokhsar, D., Richardson, P.M., DeLong, E.F., 2004. Reverse methanogenesis: testing the hypothesis with environmental genomics. Science 305 (5689), 1457–1462.

Happell, J.D., Chanton, J.P., Showers, W.S., 1994. The influence of methane oxidation on the stable isotopic composition of methane emitted from Florida swamp forests. Geochim. Cosmochim. Acta 58 (20), 4377–4388.

Haroon, M.F., Hu, S., Shi, Y., Imelfort, M., Keller, J., Hugenholtz, P., Yuan, Z., Tyson, G. W., 2013. Anaerobic oxidation of methane coupled to nitrate reduction in a novel archaeal lineage. Nature 500 (7464), 567–570.

Hinrichs, K.U., Boetius, A., 2002. The anaerobic oxidation of methane: new insights in microbial ecology and biogeochemistry. In: Ocean Margin Systems. Springer, Berlin, Heidelberg, pp. 457–477.

Hinrichs, K.U., Hayes, J.M., Sylva, S.P., Brewer, P.G., DeLong, E.F., 1999. Methane-consuming archaebacteria in marine sediments. Nature 398 (6730), 802–805.
Hoehler, T.M., Alperin, M.J., Albert, D.B., Martens, C.S., 1994. Field and laboratory studies of methane oxidation in an anoxic marine sediment: Evidence for a methanogen-sulfate reducer consortium. Global Biogeochem. Cycles 8 (4), 451–463.
House, C.H., Wong, G.M., Webster, C.R., Flesch, G.J., Franz, H.B., Stern, J.C., Pavlov, A., Atreya, S.K., Eigenbrode, J.L., Gilbert, A., Hofmann, A.E., Millan, M., Steele, A., Glavin, D.P., Malespin, C.A., Mahaffy, P.R., 2022. Depleted carbon isotope compositions observed at Gale crater, Mars. Proc. Natl. Acad. Sci. 119 (4), e2115651119. DOI: 10.1073/pnas.2115651119.
Inagaki, F., Nunoura, T., Nakagawa, S., Teske, A., Lever, M., Lauer, A., Suzuki, M., Takai, K., Delwiche, M., Colwell, F.S., Nealson, K.H., Horikoshi, K., D'Hondt, S., Jørgensen, B.B., 2006. Biogeographical distribution and diversity of microbes in methane hydrate-bearing deep marine sediments on the Pacific Ocean Margin. Proc. Natl. Acad. Sci. 103 (8), 2815–2820.
Holler, T., Wegener, G., Niemann, H., Deusner, C., Ferdelman, T.G., Boetius, A., Brunner, B., Widdel, F., 2011. Carbon and sulfur back flux during anaerobic microbial oxidation of methane and coupled sulfate reduction. Proceed. National Academy Sci. 108 (52), E1484–E1490.
Ijiri, A., Inagaki, F., Kubo, Y., Adhikari, R.R., Hattori, S., Hoshino, T., Ono, S., 2018. Deep-biosphere methane production stimulated by geofluids in the Nankai accretionary complex. Sci. Adv. 4 (6), eaao4631.
Inagaki, F., Hinrichs, K.U., Kubo, Y., Bowles, M.W., Heuer, V.B., Hong, W.L., Hoshino, T., Ijiri, A., Imachi, H., Ito, M., Kaneko, M., Lever, M.A., Lin, Y.S., Methé, B.A., Morita, S., Morono, Y., Tanikawa, W., Bihan, M., Bowden, S.A., Elvert, M., Glombitza, C., Gross, D., Harrington, G.J., Hori, T., Li, K., Limmer, D., Liu, C.H., Murayama, M., Ohkouchi, N., Ono, S., Park, Y.S., Phillips, S.C., Prieto-Mollar, X., Purkey, M., Riedinger, N., Sanada, Y., Sauvage, J., Snyder, G., Susilawati, R., Takano, Y., Tasumi, E., Terada, T., Tomaru, H., Trembath-Reichert, E., Wang, D.T., Yamada, Y., 2015. Exploring deep microbial life in coal-bearing sediment down to 2.5 km belowthe ocean floor. Science 349, 420–424.
Iversen, N., Jorgensen, B.B., 1985. Anaerobic methane oxidation rates at the sulfate-methane transition in marine sediments from Kattegat and Skagerrak (Denmark) 1. Limnol. Oceanogr. 30 (5), 944–955.
Jézéquel, D., Michard, G., Viollier, E., Agrinier, P., Albéric, P., Lopes, F., Abril, G., Bergonzini, L., 2016. Carbon cycle in a meromictic crater lake: Lake Pavin, France. In: Lake Pavin. Springer, Cham, pp. 185–203.
Jørgensen, B.B., Weber, A., Zopfi, J., 2001. Sulfate reduction and anaerobic methane oxidation in Black Sea sediments. Deep Sea Res. Part I 48 (9), 2097–2120.
Jørgensen, B.B., Böttcher, M.E., Lüschen, H., Neretin, L.N., Volkov, I.I., 2004. Anaerobic methane oxidation and a deep H2S sink generate isotopically heavy sulfides in Black Sea sediments. Geochim. Cosmochim. Acta 68 (9), 2095–2118.
Kessler, J.D., Reeburgh, W.S., Southon, J., Seifert, R., Michaelis, W., Tyler, S.C., 2006. Basin-wide estimates of the input of methane from seeps and clathrates to the Black Sea. Earth Planet. Sci. Lett. 243 (3–4), 366–375.
Kinnaman, F.S., Valentine, D.L., Tyler, S.C., 2007. Carbon and hydrogen isotope fractionation associated with the aerobic microbial oxidation of methane, ethane, propane and butane. Geochim. Cosmochim. Acta 71 (2), 271–283.
Knab, N.J., Cragg, B.A., Hornibrook, E.R.C., Holmkvist, L., Pancost, R.D., Borowski, C., Parkes, R.J., Jørgensen, B.B., 2009. Regulation of anaerobic methane oxidation in sediments of the Black Sea. Biogeosciences 6 (8), 1505–1518.
Knittel, K., Lösekann, T., Boetius, A., Kort, R., Amann, R., 2005. Diversity and distribution of methanotrophic archaea at cold seeps. Appl. Environ. Microbiol. 71 (1), 467–479.
Labidi, J., Young, E.D., Giunta, T., Kohl, I.E., Seewald, J., Tang, H., Lilley, M.D., Früh-Green, G.L., 2020. Methane thermometry in deep-sea hydrothermal systems: evidence for re-ordering of doubly-substituted isotopologues during fluid cooling. Geochim. Cosmochim. Acta 288, 248–261.
Lau, M.C., Kieft, T.L., Kuloyo, O., Linage-Alvarez, B., Van Heerden, E., Lindsay, M.R., Magnabosco, C., Wang, W., Wiggins, J.B., Guo, L., Perlman, D.H., Kyin, S., Shwe, H. H., Harris, R.L., Oh, Y., Joo Yi, M., Purtschert, R., Slater, G.F., Ono, S., Wei, S., Li, L., Sherwood Lollar, B., Onstott, T.C., 2016. An oligotrophic deep-subsurface community dependent on syntrophy is dominated by sulfur-driven autotrophic denitrifiers. Proc. Natl. Acad. Sci. 113 (49), E7927–E7936.
Lehours, A.C., Evans, P., Bardot, C., Joblin, K., Gérard, F., 2007. Phylogenetic diversity of archaea and bacteria in the anoxic zone of a meromictic lake (Lake Pavin, France). Appl. Environ. Microbiol. 73 (6), 2016–2019.
Leu, A.O., Cai, C., McIlroy, S.J., Southam, G., Orphan, V.J., Yuan, Z., Hu, S., Tyson, G.W., 2020. Anaerobic methane oxidation coupled to manganese reduction by members of the Methanoperedenaceae. ISME J. 14 (4), 1030–1041.
Lopes, F., Viollier, E., Thiam, A., Michard, G., Abril, G., Groleau, A., Prévot, F., Carrias, J. F., Albéric, P., Jézéquel, D., 2011. Biogeochemical modelling of anaerobic vs. aerobic methane oxidation in a meromictic crater lake (Lake Pavin, France). App. Geochem. 26 (12), 1919–1932.
Mangenot, X., Tarantola, A., Mullis, J., Girard, J.P., Le, V.H., Eiler, J.M., 2021. Geochemistry of clumped isotopologues of CH4 within fluid inclusions in Alpine tectonic quartz fissures. Earth Planet. Sci. Lett. 561, 116792.
Marlow, J., LaRowe, D.E., Ehlmann, B.L., Amend, J.P., Orphan, V.J., 2014. The potential for biologically catalyzed anaerobic methane oxidation on ancient Mars. Astrobiology.
Martens, C.S., Albert, D.B., Alperin, M.J., 1999. Stable isotope tracing of anaerobic methane oxidation in the gassy sediments of Eckernförde Bay, German Baltic Sea. Am. J. Sci. 299 (7–9), 589–610.
Martinez-Cruz, K., Leewis, M.C., Herriott, I.C., Sepulveda-Jauregui, A., Anthony, K.W., Thalasso, F., Leigh, M.B., 2017. Anaerobic oxidation of methane by aerobic methanotrophs in sub-Arctic lake sediments. Sci. Total Environ. 607, 23–31.
Martini, A.M., Walter, L.M., Ku, T.C., Budai, J.M., McIntosh, J.C., Schoell, M., 2003. Microbial production and modification of gases in sedimentary basins: A geochemical case study from a Devonian shale gas play, Michigan basin. AAPG Bullet. 87 (8), 1355–1375.
McDonald, I.R., Bodrossy, L., Chen, Y., Murrell, J.C., 2008. Molecular ecology techniques for the study of aerobic methanotrophs. Appl. Environ. Microbiol. 74 (5), 1305–1315.
Meng, Q., Wang, X., Wang, X., Shi, B., Luo, X., Zhang, L., Lei, Y., Jiang, C., Liu, P., 2017. Gas geochemical evidences for biodegradation of shale gases in the Upper Triassic Yanchang Formation, Ordos Basin, China. Int. J. Coal Geol. 179, 139–152.
Michaelis, W., Seifert, R., Nauhaus, K., Treude, T., Thiel, V., Blumenberg, M., Knittel, K., Gieseke, A., Peterknecht, K., Pape, T., Boetius, A., Amann, R., Jorgensen, B.B., Widdel, F., Peckmann, J., Pimenov, N.V., Gulin, M.B., 2002. Microbial reefs in the Black Sea fueled by anaerobic oxidation of methane. Science 297 (5583), 1013–1015.
Michard, G., Viollier, E., Jézéquel, D., Sarazin, G., 1994. Geochemical study of a crater lake: Lake Pavin, France-Identification, location and quantification of the chemical reactions in the lake. Chem. Geol. 115 (1–2), 103–115.
Milkov, A.V., Etiope, G., 2018. Revised genetic diagrams for natural gases based on a global dataset of> 20,000 samples. Org Geochem. 125, 109–120.
Miller, H.M., Matter, J.M., Kelemen, P., Ellison, E.T., Conrad, M.E., Fierer, N., Ruchala, T., Tominaga, M., Templeton, A.S., 2016. Modern water/rock reactions in Oman hyperalkaline peridotite aquifers and implications for microbial habitability. Geochim. Cosmochim. Acta 179, 217–241.
Mogollón, J.M., Dale, A.W., Jensen, J.B., Schlüter, M., Regnier, P., 2013. A method for the calculation of anaerobic oxidation of methane rates across regional scales: an example from the Belt Seas and The Sound (North Sea-Baltic Sea transition). Geo-Mar. Lett. 33 (4), 299–310.
Norman, L.H., 2011. Is there life on... Titan? Astron. Geophys. 52 (1), 1–39.
Oehler, D.Z., Etiope, G., 2017. Methane seepage on Mars: where to look and why. Astrobiology 17 (12), 1233–1264.
Okumura, T., Kawagucci, S., Saito, Y., Matsui, Y., Takai, K., Imachi, H., 2016. Hydrogen and carbon isotope systematics in hydrogenotrophic methanogenesis under H 2-limited and H 2-enriched conditions: implications for the origin of methane and its isotopic diagnosis. Prog. Earth Planet. Sci. 3 (1), 1–19.
Ono, S., Wang, D.T., Gruen, D.S., Sherwood Lollar, B., Zahniser, M.S., McManus, B.J., Nelson, D.D., 2014. Measurement of a doubly substituted methane isotopologue, 13CH3D, by tunable infrared laser direct absorption spectroscopy. Anal. Chem. 86 (13), 6487–6494.
Ono, S., Rhim, J.H., Gruen, D.S., Taubner, H., Kölling, M., Wegener, G., 2021. Clumped isotopologue fractionation by microbial cultures performing the anaerobic oxidation of methane. Geochim. Cosmochim. Acta 293, 70–85.
Ono, S., Rhim, J.H., Ryberg, E.C., 2022. Rate limits and isotopologue fractionations for microbial methanogenesis examined with combined pathway protein cost and isotopologue flow network models. Geochim. Cosmochim. Acta 325, 296–315.
Oremland, R.S., Taylor, B.F., 1978. Sulfate reduction and methanogenesis in marine sediments. Geochim. Cosmochim. Acta 42 (2), 209–214.
Orphan, V.J., House, C.H., Hinrichs, K.U., McKeegan, K.D., DeLong, E.F., 2001. Methane-consuming archaea revealed by directly coupled isotopic and phylogenetic analysis. Science 293 (5529), 484–487.
Oswald, K., Milucka, J., Brand, A., Hach, P., Littmann, S., Wehrli, B., Kuypers, M.M., Schubert, C.J., 2016. Aerobic gammaproteobacterial methanotrophs mitigate methane emissions from oxic and anoxic lake waters. Limnol. Oceanogr. 61 (S1), S101–S118.
Pape, T., Blumenberg, M., Seifert, R., Bohrmann, G., Michaelis, W., 2008. Marine methane biogeochemistry of the Black Sea: a review. Links Between Geolo. Proc. Microb. Activ. Evolut. Life, 281–311.
Raghoebarsing, A.A., Pol, A., Van de Pas-Schoonen, K.T., Smolders, A.J., Ettwig, K.F., Rijpstra, W.I.C., Schouten, S., Sinninghe, J.S., Op den Camp, H.J.M., Jetten, S.M., Strous, M., 2006. A microbial consortium couples anaerobic methane oxidation to denitrification. Nature 440 (7086), 918–921.
Rasigraf, O., Vogt, C., Richnow, H.H., Jetten, M.S., Ettwig, K.F., 2012. Carbon and hydrogen isotope fractionation during nitrite-dependent anaerobic methane oxidation by Methylomirabilis oxyfera. Geochim. Cosmochim. Acta 89, 256–264.
Reeburgh, W.S., 2007. Oceanic methane biogeochemistry. Chem. Rev. 107 (2), 486–513.
Reeburgh, W.S., Ward, B.B., Whalen, S.C., Sandbeck, K.A., Kilpatrickt, K.A., Kerkhof, L. J., 1991. Black Sea methane geochemistry. Deep Sea Res. Part A Oceanogr. Res. Papers 38, S1189–S1210.
Ruffine, L., Deusner, C., Haeckel, M., Kossel, E., Toucanne, S., Chéron, S., Boissier, A., Schmidt, M., Donval, J-P., Scholz, F., Guyader, V., Ker, S., Riboulot, V., 2021. Effects of postglacial seawater intrusion on sediment geochemical characteristics in the Romanian sector of the Black Sea. Marine and Petroleum Geology 123, 104746.
Russell, M.J., Nitschke, W., 2017. Methane: fuel or exhaust at the emergence of life? Astrobiology 17 (10), 1053–1066.
Schoell, M., 1988. Multiple origins of methane in the Earth. Chem. Geol. 71 (1–3), 1–10.
Schubert, C.J., Coolen, M.J., Neretin, L.N., Schippers, A., Abbas, B., Durisch-Kaiser, E., Wehrli, B., Hopmans, E.C., Sinninghe Damsté, J.S., Wakeham, S., Kuypers, M.M., 2006. Aerobic and anaerobic methanotrophs in the Black Sea water column. Environ. Microbiol. 8 (10), 1844–1856.

Schubert, C.J., Vazquez, F., Lösekann-Behrens, T., Knittel, K., Tonolla, M., Boetius, A., 2011. Evidence for anaerobic oxidation of methane in sediments of a freshwater system (Lago di Cadagno). FEMS Microbiol. Ecol. 76 (1), 26–38.
Seeberg-Elverfeldt, J., Schlüter, M., Feseker, T., Kölling, M., 2005. Rhizon sampling of porewaters near the sediment-water interface of aquatic systems. Limnol. Oceanogr. Methods 3 (8), 361–371.
Sherwood Lollar, B., Frape, S.K., Weise, S.M., Fritz, P., Macko, S.A., Welhan, J.A., 1993. Abiogenic methanogenesis in crystalline rocks. Geochim. Cosmochim. Acta 57 (23–24), 5087–5097.
Simkus, D.N., Slater, G.F., Lollar, B.S., Wilkie, K., Kieft, T.L., Magnabosco, C., Lau, M.C. Y., Pullin, M.J., Hendrickson, S.B., Wommack, K.E., Sakowski, E.G., van Heerden, E., Kuloyo, O., Linage, B., Borgonie, G., Onstott, T.C., 2016. Variations in microbial carbon sources and cycling in the deep continental subsurface. Geochim. Cosmochim. Acta 173, 264–283.
Stolper, D.A., Sessions, A.L., Ferreira, A.A., Neto, E.S., Schimmelmann, A., Shusta, S.S., Valentine, D.L., Eiler, J.M., 2014a. Combined ^{13}C–D and D-D clumping in methane: Methods and preliminary results. Geochim. Cosmochim. Acta 126, 169–191.
Stolper, D.A., Lawson, M., Davis, C.L., Ferreira, A.A., Neto, E.S., Ellis, G.S., Lewan, M.D., Martini, A.M., Tang, Y., Schoell, M., Sessions, A.L., Eiler, J.M., 2014b. Formation temperatures of thermogenic and biogenic methane. Science 344 (6191), 1500–1503.
Stolper, D.A., Martini, A.M., Clog, M., Douglas, P.M., Shusta, S.S., Valentine, D.L., Sessions, A.L., Eiler, J.M., 2015. Distinguishing and understanding thermogenic and biogenic sources of methane using multiply substituted isotopologues. Geochim. Cosmochim. Acta 161, 219–247.
Stolper, D.A., Lawson, M., Formolo, M.J., Davis, C.L., Douglas, P.M., Eiler, J.M., 2017. The utility of methane clumped isotopes to constrain the origins of methane in natural gas accumulations Special Publications Geol. Soc. Lond. 468, SP468-3.
Summons, R.E., Jahnke, L.L., Roksandic, Z., 1994. Carbon isotopic fractionation in lipids from methanotrophic bacteria: relevance for interpretation of the geochemical record of biomarkers. Geochim. Cosmochim. Acta 58 (13), 2853–2863.
Swart, P.K., 1991. The oxygen and hydrogen isotopic composition of the Black Sea. Deep Sea Res. Part A Oceanogr. Res. Papers 38, S761–S772.
Taenzer, L., Labidi, J., Masterson, A.L., Feng, X., Rumble III, D., Young, E.D., Leavitt, W. D., 2020. Low $\Delta^{12}CH_2D_2$ values in microbialgenic methane result from combinatorial isotope effects. Geochim. Cosmochim. Acta 285, 225–236.
Templeton, A.S., Chu, K.H., Alvarez-Cohen, L., Conrad, M.E., 2006. Variable carbon isotope fractionation expressed by aerobic CH4-oxidizing bacteria. Geochimica et Cosmochimica Acta 70 (7), 1739–1752.
Timmers, P.H., Welte, C.U., Koehorst, J.J., Plugge, C.M., Jetten, M.S., Stams, A.J., 2017. Reverse methanogenesis and respiration in methanotrophic archaea. Archaea 2017.
Treude, T., Knittel, K., Blumenberg, M., Seifert, R., Boetius, A., 2005. Subsurface microbial methanotrophic mats in the Black Sea. Appl. Environ. Microbiol. 71 (10), 6375–6378.
Trotsenko, Y.A., Murrell, J.C., 2008. Metabolic aspects of aerobic obligate methanotrophy★. Adv. Appl. Microbiol. 63, 183–229.
Valenzuela, E.I., Prieto-Davó, A., López-Lozano, N.E., Hernández-Eligio, A., Vega-Alvarado, L., Juárez, K., Garcia-Gonzalez, A.S., Lopez, M.G., Cervantes, F.J., 2017. Anaerobic methane oxidation driven by microbial reduction of natural organic matter in a tropical wetland. Appl. Environ. Microbiol. 83 (11), e00645–e717.
Viollier, E., Michard, G., Jézéquel, D., Pèpe, M., Sarazin, G., 1997. Geochemical study of a crater lake: Lake Pavin, Puy de Dôme, France. Constraints afforded by the particulate matter distribution in the element cycling within the lake. Chem. Geol. 142 (3–4), 225–241.
Wakeham, S.G., Lewis, C.M., Hopmans, E.C., Schouten, S., Damsté, J.S.S., 2003. Archaea mediate anaerobic oxidation of methane in deep euxinic waters of the Black Sea. Geochim. Cosmochim. Acta 67 (7), 1359–1374.
Wang, D.T., Reeves, E.P., McDermott, J.M., Seewald, J.S., Ono, S., 2018. Clumped isotopologue constraints on the origin of methane at seafloor hot springs. Geochim. Cosmochim. Acta 223, 141–158.
Wang, D.T., Gruen, D.S., Sherwood Lollar, B., Hinrichs, K.U., Stewart, L.C., Holden, J.F., Hristov, A.N., Pohlman, J.W., Morrill, P.L., Konneke, M., Delwiche, K.B., Reeves, E. P., Sutcliffe, C.N., Ritter, D.J., Seewald, J.S., McInstosh, J.C., Hemond, H.F., Kubo, M.D., Cardace, D., Hoehler, T.M., Ono, S., 2015. Nonequilibrium clumped isotope signals in microbial methane. Science 348 (6233), 428–431.
Wang, Z., Schauble, E.A., Eiler, J.M., 2004. Equilibrium thermodynamics of multiply substituted isotopologues of molecular gases. Geochim. Cosmochim. Acta 68 (23), 4779–4797.
Wang, D.T., Welander, P.V., Ono, S., 2016. Fractionation of the methane isotopologues $^{13}CH_4$, $^{12}C_H3D$, and $^{13}C_H3D$ during aerobic oxidation of methane by Methylococcus capsulatus (Bath). Geochim. Cosmochim. Acta 192, 186–202.
Ward, J.A., Slater, G.F., Moser, D.P., Lin, L.H., Lacrampe-Couloume, G., Bonin, A.S., Davidson, M., Hall, J.A., Mislowack, B., Bellamy, R.E.S., Onstott, T.C., Sherwood Lollar, B., 2004. Microbial hydrocarbon gases in the Witwatersrand Basin, South Africa: implications for the deep biosphere. Geochim. Cosmochim. Acta 68 (15), 3239–3250.
Warr, O., Young, E.D., Giunta, T., Kohl, I.E., Ash, J.L., Lollar, B.S., 2021. High-resolution, long-term isotopic and isotopologue variation identifies the sources and sinks of methane in a deep subsurface carbon cycle. Geochim. Cosmochim. Acta 294, 315–334.
Weber, H.S., Habicht, K.S., Thamdrup, B., 2017. Anaerobic methanotrophic archaea of the ANME-2d cluster are active in a low-sulfate, iron-rich freshwater sediment. Front. Microbiol. 8, 619.
Webster, G., Sass, H., Cragg, B.A., Gorra, R., Knab, N.J., Green, C.J., Mathes, F., Fry, J.C., Weightman, A.J., Parkes, R.J., 2011. Enrichment and cultivation of prokaryotes associated with the sulphate–methane transition zone of diffusion-controlled sediments of Aarhus Bay, Denmark, under heterotrophic conditions. FEMS Microbiol. Ecol. 77 (2), 248–263.
Wegener, G., Gropp, J., Taubner, H., Halevy, I., Elvert, M., 2021. Sulfate-dependent reversibility of intracellular reactions explains the opposing isotope effects in the anaerobic oxidation of methane. *Science*. Advances 7 (19), eabe4939.
Weiss, M.C., Sousa, F.L., Mrnjavac, N., Neukirchen, S., Roettger, M., Nelson-Sathi, S., Martin, W.F., 2016. The physiology and habitat of the last universal common ancestor. Nat. Microbiol. 1 (9), 1–8.
Whitehill, A.R., Joelsson, L.M.T., Schmidt, J.A., Wang, D.T., Johnson, M.S., Ono, S., 2017. Clumped isotope effects during OH and Cl oxidation of methane. Geochim. Cosmochim. Acta 196, 307–325.
Whiticar, M.J., 1999. Carbon and hydrogen isotope systematics of bacterial formation and oxidation of methane. Chem. Geol. 161 (1–3), 291–314.
Xia, X., Gao, Y., 2019. Kinetic clumped isotope fractionation during the thermal generation and hydrogen exchange of methane. Geochim. Cosmochim. Acta 248, 252–273.
Yamamoto, S., Alcauskas, J.B., Crozier, T.E., 1976. Solubility of methane in distilled water and seawater. J. Chem. Eng. Data 21 (1), 78–80.
Yoshinaga, M.Y., Holler, T., Goldhammer, T., Wegener, G., Pohlman, J.W., Brunner, B., Kuypers, M.M.M., Hinrichs, K., Elvert, M., 2014. Carbon isotope equilibration during sulphate-limited anaerobic oxidation of methane. Nat. Geosci. 7 (3), 190–194.
Young, E.D., 2019. A two-dimensional perspective on CH4 isotope clumping. Deep Carbon: Past to Present, pp. 388–414.
Young, E.D., Rumble III, D., Freedman, P., Mills, M., 2016. A large-radius high-mass-resolution multiple-collector isotope ratio mass spectrometer for analysis of rare isotopologues of O2, N2, CH4 and other gases. Int. J. Mass Spectrom. 401, 1–10.
Young, E.D., Kohl, I.E., Sherwood Lollar, B., Etiope, G., Rumble, D., Li, S., Haghnegahdar, M.A., Schauble, E.A., McCain, K.A., Foustoukos, D.I., Sutclife, C., Warr, O., Ballentine, C.J., Onstott, T.C., Hosgormez, H., Neubeck, A., Marques, J. M., Pérez-Rodriguez, I., Rowe, A.R., LaRowe, D.E., Magnabosco, C., Yeung, L.Y., Ash, J.L., Bryndzia, L.T., 2017. The relative abundances of resolved $^{12}CH_2D_2$ and $^{13}CH_3D$ and mechanisms controlling isotopic bond ordering in abiotic and biotic methane gases. Geochim. Cosmochim. Acta 203, 235–264.
Zhang, N., Snyder, G.T., Lin, M., Nakagawa, M., Gilbert, A., Yoshida, N., Matsumoto, R., Sekine, Y., 2021. Doubly substituted isotopologues of methane hydrate ($^{13}CH_3D$ and $^{12}CH_2D_2$): Implications for methane clumped isotope effects, source apportionments and global hydrate reservoirs. Geochim. Cosmochim. Acta 315, 127–151.
Zhou, Z., Liu, Y., Lloyd, K.G., Pan, J., Yang, Y., Gu, J.D., Li, M., 2019. Genomic and transcriptomic insights into the ecology and metabolism of benthic archaeal cosmopolitan, Thermoprofundales (MBG-D archaea). ISME J. 13 (4), 885–901.